nature chemical engineering

Article

https://doi.org/10.1038/s44286-024-00125-2

Flash separation of metals by electrothermal chlorination

Received: 7 March 2024

Accepted: 29 August 2024

Published online: 25 September 2024

Check for updates

Bing Deng[1,2,7] ✉, Shichen Xu[1,7], Lucas Eddy[1,3], Jaeho Shin[1], Yi Cheng[1], Carter Kittrell[1], Khalil JeBailey[4], Justin Sharp[1], Long Qian[1], Shihui Chen[1] & James M. Tour[1,4,5,6] ✉

Metal recycling plays a crucial role in mitigating the shortage of critical metals and reducing reliance on primary mining. Current liquid hydrometallurgy involves substantial water and chemical consumption with troublesome secondary waste streams, while pyrometallurgy lacks selectivity and requires substantial energy input. Here we develop an electrothermal chlorination and carbochlorination process, and a specialized compact reactor, for the selective separation of individual critical metals from electronic waste. Our approach uses programmable, pulsed current input to achieve precise control over a wide temperature range (from room temperature to 2,400 °C), short reaction durations of seconds and rapid heating/cooling rates (10^3 °C s^{-1}) during the process. The method capitalizes on the differences in the free energy formation of the metal chlorides. Once conversion to a specific metal chloride is achieved, that compound distills from the mixture in seconds. This allows both thermodynamic and kinetic selectivity for desired metals with minimization of impurities.

There is a pressing demand for metals in various electronic applications, superalloys and renewable energy systems[1,2]. Critical metals, aptly named for their importance in emerging technologies, are becoming harder to access and pose potential risks to the supply chain[3]. Within the electronics industry, representative critical metals include indium (In), gallium (Ga) and tantalum (Ta), which find widespread applications in displays, semiconductors, lighting and capacitors. For example, In, predominantly recovered from by-product residues during copper and zinc production[4], is indispensable for producing indium tin oxide (ITO) thin films, an essential component of transparent electrodes in displays and touch screens. Similarly, Ga, obtained as a by-product of commodity metal production[5], is used in semiconductor forms such as gallium arsenide (GaAs), gallium nitride (GaN) and aluminum gallium indium phosphide (AlGaInP). Ta is extensively employed in capacitors for cellular phones and computers[6], constituting 34% of total Ta consumption[7]. With the increasing demand for personal electronics, the consumption of these critical metals is experiencing a sharp rise and previous supply chain dependability is ending[8]. Recovering critical metals from electronics at their end of life[9] falls under the realm of urban mining[10], thereby averting disruptions in the critical materials supply chains while mitigating the environmental impact of traditional mining and electronic waste (e-waste) disposal[11].

Metals, in theory, are infinitely recyclable[12]. However, current metal recycling and separation is inefficient due to the complexity of product design and restrictions on recycling technologies[13]. Conventional hydrometallurgical processes[14], involving acid/alkaline leaching and liquid–liquid separation such as solvent extraction, exhibit good selectivity but are marked by substantial water and chemical consumption, often leading to the generation of secondary wastewater streams[15]. Classical pyrometallurgical processes often lack selectivity, and the accumulation of alloying elements can result in the downgrading of metals[16]. Recently, a selective sulfidation was demonstrated to separate metals from a mixed metal oxide feedstock[17].

[1]Department of Chemistry, Rice University, Houston, TX, USA. [2]School of Environment, Tsinghua University, Beijing, China. [3]Applied Physics Program, Rice University, Houston, TX, USA. [4]Department of Materials Science and NanoEngineering, Rice University, Houston, TX, USA. [5]Smalley-Curl Institute, Rice University, Houston, TX, USA. [6]NanoCarbon Center and the Rice Advanced Materials Institute, Rice University, Houston, TX, USA. [7]These authors contributed equally: Bing Deng, Shichen Xu. ✉e-mail: dengbing@tsinghua.edu.cn; tour@rice.edu

The chlorination process, commonly employed in extractive metallurgy for metal separations, has been used industrially to separate titanium (Ti) from its ores[18]. This process involves the reaction of various metals or metal compounds with chlorinating agents to form metal chlorides[19,20]. Commercially, chlorination is conducted using fluidized bed[21], typically operating within a temperature range of 900–1,300 °C (ref. 22). However, this limited temperature range restricts its wide applicability. Consequently, the chlorination process is employed practically in specific scenarios, such as for obtaining Ti and magnesium (Mg)[19]. In addition, chlorination at the laboratory scale is performed using indirect furnace heating. For example, In recovery from dental metal recycling sludges[23] and Ga recovery from solar cell waste materials[24] with ammonium chloride as the chlorinating agents has been described. The sluggish heating/cooling processes and long treatment durations inherent in indirect heating reduce the energy efficiency and production rate of metal recovery, usually resulting in less economic incentives for use.

In addressing these limitations, we introduce direct electric heating[25,26] or flash heating[27], characterized by ultrafast heating/cooling, rapid treatment, and widely tunable temperature, into the chlorination process. This integration is termed as electrothermal chlorination (ETC), and electrothermal carbochlorination (ETCC) when carbon is used as a reductant additive. These features enable us to overcome the constraints of the conventional chlorination process, substantially expanding its applicability in metals recovery and separation, increasing the production rate and lowering the energy consumption. This is evidenced by the successful high-yield and high-purity recovery of In, Ga and Ta from authentic e-wastes.

Results

Thermodynamic basis and setup

In our initial phase, we undertook a thermodynamic analysis of the chlorination reactions of 34 metal oxides, using chlorine (Cl_2) as the chlorinating agent. This comprehensive study covered representative metals across *s*, *p* and *d* blocks of the Periodic Table (Fig. 1a, Supplementary Note 1 and Supplementary Data 1). Both the chlorination reaction (equation (1)) and carbochlorination reaction (equation (2)) were calculated:

$$MO_x + xCl_2 = MCl_{2x} + x/2O_2 \quad (1)$$

$$MO_x + xCl_2 + xC = MCl_{2x} + xCO \quad (2)$$

These reactions fall into four groups based on their spontaneity under various temperature conditions: (1) the chlorination reaction is spontaneous at any temperature >0 °C; (2) the chlorination reaction is spontaneous with a lower limit temperature threshold (T_{crit}); (3) the chlorination reaction is spontaneous with an upper limit temperature threshold; (4) the chlorination reaction is not spontaneous under any readily accessible temperature but its carbochlorination reaction is spontaneous, where carbon serves as a reductant. This analysis reveals limitations in the conventional chlorination reaction. First, the temperature required for chlorination reactions can range from 400 to 2,400 °C; thus, many metal oxides cannot be chlorinated using a conventional furnace generally operating under 1,500 °C. Second, the reaction temperature difference is narrow among some metal oxides, in which cases precise temperature control is required for the reactivity-based separation. Third, for metals with similar chlorination reactivity trends, it is challenging to separate them solely on the basis of thermodynamics.

To overcome these obstacles, we introduced direct electric heating, proposing the ETC and ETCC processes (Fig. 1b and Extended Data Fig. 1a). Diverging from conventional furnaces that use thermal convection, our method employs a carbon paper heater platform to heat the feedstock through thermal conduction. We built an electrical system (Extended Data Fig. 1b,c) to deliver programmable current input to the heater (Fig. 1c), allowing rapid heating and cooling within seconds (Fig. 1d). The heater temperature can be precisely regulated through voltage input variation (Extended Data Fig. 1c), enabling a wide temperature range, from 400 to 2,500 °C (Fig. 1e,f). The maximum temperature is mainly controlled by the voltage input. ETC/ETCC presents several improved features that address conventional furnace heating limitations. First, the high temperature capability up to 2,500 °C (Fig. 1f) permits chlorination for almost all metal oxides (Fig. 1a). Second, precise temperature control by just tuning the voltage input (Fig. 1f) facilitates the separation of metals with a narrow reaction window. Third, the precise temperature control would also contribute to metal separation based upon vapor pressure difference of chlorides (Extended Data Fig. 2). Lastly, rapid heating (up to ~4,500 °C s^{-1}) and cooling (~500 °C s^{-1}) rates (Fig. 1f) permit kinetic selectivity, allowing reactions with similar thermodynamics profiles to be distinguished on the basis of their rates and activation energy differences.

In the ETC/ETCC configuration, metal oxide precursors (mixed with carbon for ETCC) and Cl_2 gas underwent heating by the carbon paper heater. To elucidate the details of the sample and surrounding Cl_2 gas heating process dynamics, we conducted simulations based on the finite element method using the heat transfer module in solid and fluid interfaces (see details in Supplementary Note 2, Supplementary Tables 1 and 2 and Extended Data Fig. 3a,b). The carbon paper transfers heat to the solid sample and the chlorine gas through conduction and convection, respectively. We fixed the heater temperature at T_{heater} = 1,141 °C, which is the experimentally measured value under voltage input of U = 60 V (Fig. 1f). The sample and gas temperatures reach a plateau (~1,141 °C) within ~4 s (Fig. 1g and Extended Data Fig. 3c), in contrast to traditional indirect heating processes taking hours to achieve thermal balance, highlighting the rapid heating capability of the electrothermal process. This rapid heat transfer suggests the chlorination reaction is operating primarily under a thermodynamic equilibrium. By varying the T_{heater}, the sample and gas temperatures closely follow the T_{heater} pattern (Fig. 1h and Extended Data Fig. 3d), showcasing the precise reaction temperature controllability. Having established the underlying thermodynamics, designed the equipment and clarified heat transfer details, we transitioned to case studies focusing on recovery and separation of critical metals from authentic e-wastes.

In recovery from ITO-containing waste

In holds a crucial status as a technology-critical element, primarily employed in ITO, which therefore becomes the main waste for In recycling[28]. ITO is composed of 90% In and 10% tin (Sn) in their oxide forms. We analyzed the thermodynamics of the chlorination reaction of In_2O_3 and SnO_2 using Cl_2 as the chlorinating agent (Fig. 2a). Within a temperature window of 630–1,240 °C, In_2O_3 converts to $InCl_3$, while SnO_2 remains unreacted. This allows the immediate evaporation of $InCl_3$ (boiling point (b.p.), 497 °C) as the volatile phase, facilitating the separation from SnO_2 (sublimes, 1,800 °C) based on their volatility difference. The corresponding voltage input range is between 90 and 110 V (Fig. 2b and Supplementary Fig. 1).

To validate our approach, we controlled the voltage input at 100 V, demonstrating the feasibility of converting In_2O_3 to $InCl_3$ through the ETC process (Extended Data Fig. 4a,b). Then, we used raw ITO as the precursor. After the ETC process, we obtained volatiles condensed on the quartz tube and residues remaining on the heater (Fig. 2c). Raman spectra and X-ray diffraction (XRD) patterns identified the volatiles as $InCl_3$ and the residue as SnO_2 (Fig. 2d,e). We further investigated the impact of voltage input on purity and yield (Fig. 2f). As voltage increases, the yield is improved due to the more complete reaction; however, excessive voltage input at 120 V leads to reduced purity because of the concurrent chlorination of SnO_2 (Fig. 2b).

https://doi.org/10.1038/s44286-024-00125-2

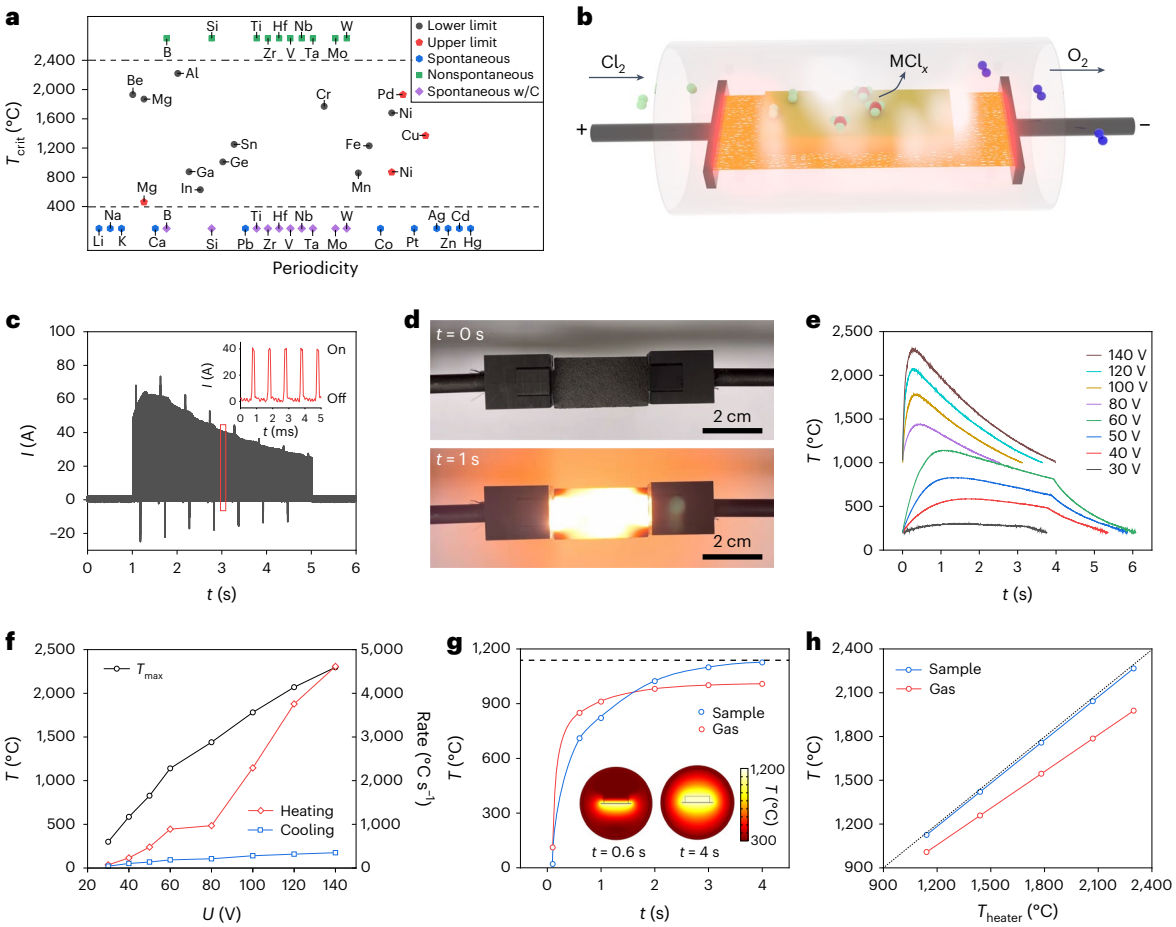

Fig. 1 | Thermodynamic analysis and setup of the ETC/ETCC process. a, The calculated critical reaction (w/C, with carbon) temperature (T_{crit}) of chlorination and carbochlorination for various metal oxides. The dashed lines denote the temperatures at 400 °C and 2,400 °C. **b**, Schematic of the ETC/ETCC process showing the metal chlorides vaporize and deposit on the surrounding quartz tube. **c**, The measured current profile at 60 V, heater resistance of ~1 Ω and pulse duty cycle of 10%. Inset: the enlarged current profile in the red rectangle. **d**, Pictures of the heater before (top) and during (bottom) electric heating. **e**, The measured temperature profiles of the heater under different voltage inputs. **f**, The measured maximum temperature (T_{max}) and heating/cooling rates of the heater under different voltage inputs. **g**, Simulated temperature profiles of the sample and gas. The sample temperature is defined as its average temperature, and the gas temperature as the average of the gas within the diameter of carbon paper heater width, considering that only the gas close to the sample reacts. The dashed line denotes the heater temperature, which is fixed at 1,141 °C, corresponding to the maximum temperature at 60 V input. Inset: the simulated cross-sectional temperature distribution at t = 0.6 s and 4 s. **h**, The correlation of simulated sample and gas temperature versus the heater temperature (T_{heater}).

The optimized result exhibits 99% purity and 91% yield of In in the volatile product (Fig. 2f). The recovery yield can be further improved by adding carbon separators to retard the gas-phase loss of the desired product (Extended Data Fig. 4c,d).

Transitioning to authentic e-waste, we focused on the recovery of In from used transparent conductive films (TCF). After removing plastic substrates by calcination (Extended Data Fig. 4e–h), the resulting metal mixture primarily composed of Au, In, Sn, Mn and Cr, among others. Total quantification through digestion followed by inductively coupled plasma mass spectrometry (ICP-MS) measurement indicated that In accounts for ~30 wt% among the metal content (Fig. 2g). We considered five primary metals with content >1 wt%: Au, In, Sn, Mn and Cr. Computational thermodynamic analysis of the chlorination reaction was conducted on Au, In_2O_3, SnO_2, MnO and Cr_2O_3 (Fig. 2h). Within a temperature window of 630–830 °C, only In_2O_3 would be chlorinated and separated from other metals through evaporation (Extended Data Fig. 4i). The effect of voltage input on In recycling performance was investigated (Fig. 2i and Extended Data Fig. 4j,k). An insufficiently low voltage at 100 V led to inadequate temperature, chlorinating Au along with In_2O_3, resulting in low In product purity. Conversely, excessively high voltage input at 110 V caused the chlorination of SnO_2 and MnO, reducing the desired In product purity. At an optimal voltage of 105 V, the best overall performance was achieved, with 95% purity and 92% yield of In (Fig. 2i). This underscores the pivotal role of careful temperature control in the selective recovery of metals, a notable advantage of the ETC process.

Ga recovery from LED manufacturing wastes

The recovery of Ga from e-wastes offers an alternative solution to counterbalance the escalating demand for Ga in consumer electronics. We first used neat GaN to exemplify the feasibility of ETC (Supplementary Fig. 2). Then, we used light-emitting diode (LED) manufacturing wastes as the resource for Ga recovery (Methods and Extended Data Fig. 5). After removing the silicon substrate, we obtained a mixed metal powder predominantly composed of Ag, SiO_2, Au and GaN, with Ga constituting ~30 wt% among the metal contents.

Thermodynamic analysis revealed that the chlorination of Ag and GaN is spontaneous over a wide range of temperatures, while SiO_2 and Au chlorination reaction is not spontaneous at temperatures >290 °C (Extended Data Fig. 6a). Despite the lack of

https://doi.org/10.1038/s44286-024-00125-2

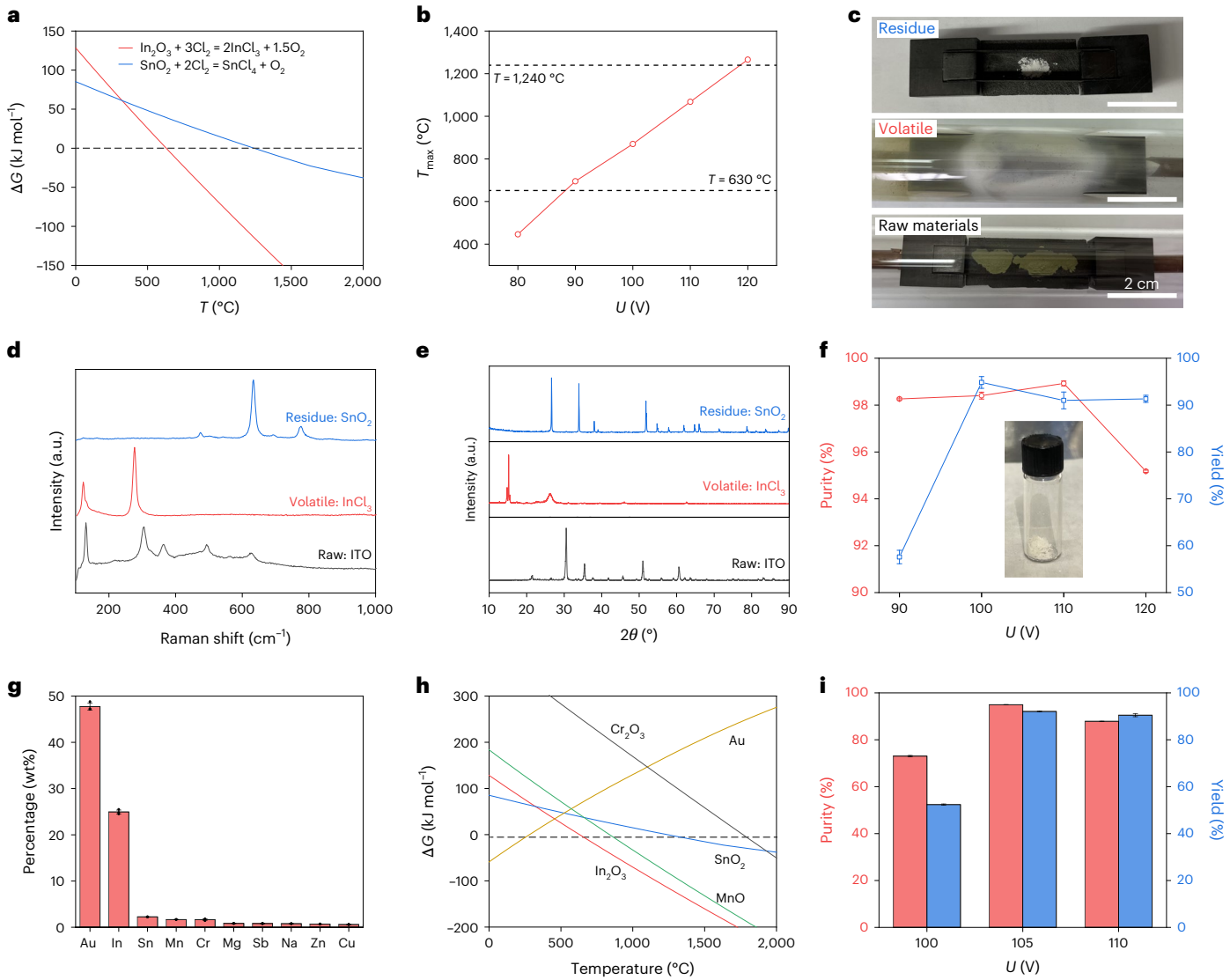

Fig. 2 | Selective recovery of In from ITO-containing waste. a, The calculated ΔG versus temperature for chlorination of In_2O_3 and SnO_2. The dashed line denotes $\Delta G = 0$ kJ mol^{-1}. **b**, The maximum temperature (T_{max}) of the carbon paper heater versus voltage input with the duty cycle of 5%. The bottom and top dashed lines denote $T = 630$ °C and 1,240 °C, respectively. **c**, A picture of the ITO raw material (bottom), the volatile (middle) and the residue (top). **d**, Raman spectra of the ITO raw material, $InCl_3$ volatile product and SnO_2 residue. **e**, XRD patterns of the ITO raw material (powder diffraction file (PDF) #01-089-4597), $InCl_3$ volatile product (PDF #01-0170) and SnO_2 residue (PDF# 00-021-1250). The broad peak at 26.3° is ascribed to Kapton tape used to seal the $InCl_3$ sample to slow its deliquescence. **f**, The purity and yield of the product versus voltage input. Inset: a picture of the $InCl_3$ obtained. **g**, The major metal composition in the TCF waste. **h**, ΔG of chlorination reaction versus temperature for main components in the TCF waste, including In_2O_3, MnO, SnO_2, Au and Cr_2O_3. The dashed line denotes $\Delta G = 0$ kJ mol^{-1}. **i**, The recovery yield and purity of In from the TCF waste. The error bars in **f**, **g** and **i** denote the standard deviation where the measurement replicate is $N = 3$.

thermodynamic differentiation between Ag and GaN chlorination, their chloride products, AgCl (b.p., 1,550 °C) and $GaCl_3$ (b.p., 201 °C), exhibit notable differences in vapor pressure (Extended Data Fig. 6b), thereby ensuring their separation. ETC followed by selective evaporation from LED manufacturing wastes (Extended Data Fig. 6c), through an optimized voltage input, afforded Ga with 97.5% purity and 86.4% yield (Extended Data Figs. 6d,e). The near absence of Ga in the residue confirmed the completeness of the reaction (Extended Data Fig. 6f–i). Secondary wastewater streams and tailings are mitigated.

Ta recovery from waste capacitors

Ta is another technology-critical metal, primarily integral to electronic components as capacitors[29]. The vast prevalence of Ta capacitor waste (TCW) in used small electrical appliances, with a high Ta content up to 45 wt%, positions them as a high-grade Ta resource[30]. Before the ETC/ETCC recovery, the raw TCW was subjected to calcination in air to eliminate plastic and resin layers. This process yielded a finely powdered mixture, dominated by various metal oxides, including tantalum pentoxide (Ta_2O_5; Supplementary Fig. 3). Total quantification of metals in the powder discloses that Ta constitutes 37.8 wt% among metal contents, accompanied by other notable metal compositions (>1 wt%), including Si, Mn, Cu, Fe and Ni (Fig. 3a).

Computational thermodynamic analysis of the chlorination reactions for these metal oxides with Cl_2 delineated two groups (Fig. 3b): (1) CuO, Fe_2O_3, NiO and MnO, with spontaneous chlorination reactions with specific temperature thresholds; and (2) Ta_2O_5 and SiO_2, with thermodynamically unfavorable chlorination reactions. Experimental verification through ETC of Ta_2O_5 with Cl_2 corroborated it as being unreactive (Supplementary Fig. 4). For Ta_2O_5 and SiO_2, the thermodynamics

https://doi.org/10.1038/s44286-024-00125-2

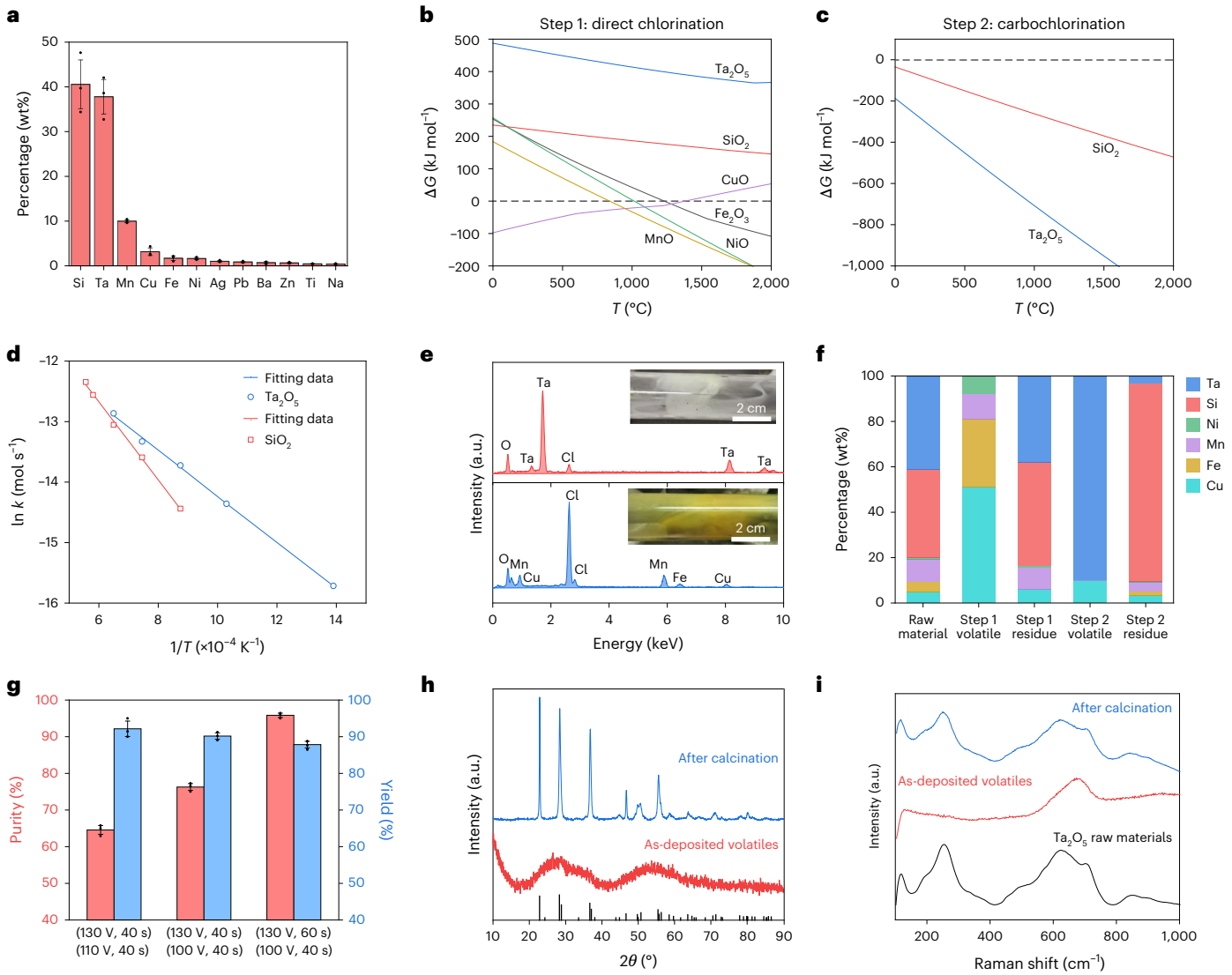

Fig. 3 | Selective recovery of Ta from TCW. a, The major metals present in the TCW. **b**, ΔG of the chlorination reaction versus temperature for major metals in TCW, including Ta_2O_5, SiO_2, CuO, Fe_2O_3, NiO and MnO. The dashed line denotes $\Delta G = 0$ kJ mol^{-1}. **c**, ΔG of the carbochlorination reaction versus temperature for Ta_2O_5 and SiO_2. The dash line denotes $\Delta G = 0$ kJ mol^{-1}. **d**, The kinetics of the carbochlorination of Ta_2O_5 and SiO_2. The slopes of the fitted curves according to the Arrhenius equation where the activation energies are 53.6 kJ mol^{-1} for SiO_2 and 31.6 kJ mol^{-1} for Ta_2O_5. **e**, EDS spectra of the first-step volatile (bottom) and the second-step volatile (top). Insets are the pictures of the volatiles condensed on the quartz tube: step 1 chlorination (bottom inset) and step 2 carbochlorination (top inset). **f**, Metal content percentages in TCW raw materials, step 1 chlorination volatile and residue, and step 2 carbochlorination volatile and residue. **g**, The product purity and yield under different ETC conditions. The first row on the *x* axis denotes the first step ETC parameters, and the second row denotes the second step ETCC parameters. **h**, XRD patterns of the as-deposited volatiles and that after calcination. The reference PDF of Ta_2O_5 is shown (01-082-9637). **i**, Raman spectra of the Ta_2O_5 raw materials, as-deposited volatiles and that after calcination. The error bars in **a** and **g** denote standard deviation where the measurement replicate is $N = 3$.

of their carbochlorination reactions were analyzed (Fig. 3c), revealing thermodynamic spontaneity for both oxides by ETCC. Despite the thermodynamic similarity, the substantial difference in Gibbs free energy change (ΔG) between SiO_2 and Ta_2O_5 suggests possible kinetic selectivity for their separation. To experimentally verify this, we mixed Ta_2O_5 with carbon (C) and conducted the ETCC reaction (Supplementary Fig. 5). Ta_2O_5 was successfully converted to a volatile product projected to be tantalum oxychlorides[31], which can be collected through evaporation–condensation. SiO_2 underwent a similar treatment. Carbochlorination reaction kinetics were experimentally determined for SiO_2 and Ta_2O_5, from which we obtained the rate constants (Supplementary Note 3). Based on the Arrhenius equation, the activation energies (E_a) of carbochlorination reactions were calculated to be $E_a(SiO_2) = 53.6$ kJ mol^{-1} and $E_a(Ta_2O_5) = 31.6$ kJ mol^{-1} (Fig. 3d). The activation energy difference facilitates the kinetically controlled separation of Ta_2O_5 and SiO_2. To show this, we mixed SiO_2 and Ta_2O_5 with C and conducted the ETCC reaction (Supplementary Fig. 6a). By precisely controlling the voltage at 100 V and corresponding temperature at ~1,050 °C, Ta_2O_5 was selectively chlorinated and separated by evaporation from the unreacted SiO_2 residue (Supplementary Figs. 6b,c).

Leveraging the thermodynamic and kinetic selectivity, we devised a two-step strategy for Ta separation from TCW (Supplementary Fig. 7). In the first step, the ETC reaction at 1,230–1,380 °C converted CuO, Fe_2O_3, NiO and MnO to their chlorides, which evaporated as the volatile phase. Ta_2O_5 and SiO_2 were unreactive and in the residue phase. Elemental dispersion spectroscopy (EDS; Fig. 3e, bottom and Supplementary Fig. 8) and ICP-MS (Fig. 1f, step 1 volatile and residue)

confirmed this enrichment and separation. In the second step, the ETCC reaction involved mixing the first-step residue with C and then carbochlorination reaction. By controlling the electrothermal temperature at ~1,050 °C, Ta_2O_5 was predominantly chlorinated and collected as the volatile phase (Fig. 3e, top and Fig. 3f, step 2 volatile), while SiO_2 remained predominantly in the residue (Fig. 3f, step 2 residue; Supplementary Fig. 9). After optimizing the voltage input and duration of the two-step strategy, we achieved the selective recovery of Ta from TCW with 96% purity and 88% yield (Fig. 3g). The obtained Ta product is an amorphous tantalum oxychloride, which easily converts into pure Ta_2O_5 through mild calcination in air (Fig. 3h,i).

Scale-up capability

The scalability of the ETC/ETCC process is critical for practical applications. Ensuring precise temperature control, a key factor in selective metal recovery, involves understanding the parameters influencing temperature. According to our theoretical analyses ('The critical role of heater resistance in joule heating' in Supplementary Note 4), an optimal heater resistance exists for efficient energy conversion from electricity to heat. This value is determined by the electrical supply system, and the optimized resistance range of 0.5–2.0 Ω for the carbon paper heater platform. Consistency in heater resistance is vital during the scale-up process, which can be realized by maintaining the thickness and aspect ratio (defined as ratio of length to width, L/W) of the heater platform ('Design of a carbon paper heater' in Supplementary Note 4). In our initial experiments, we used a carbon paper heater with dimensions of 3×1 cm^2 (L/W), defined as a scaling factor (S) of 1. To explore scalability, we used an enlarged heater while keeping the aspect ratio at 3. Under the same voltage input of 120 V, the larger-sized heater exhibited a lower temperature, a predictable outcome (Fig. 4a). A heat/temperature map varying with the size of the heater and the voltage input was constructed to guide the required voltage input during scale-up (Fig. 4b).

After elucidating the size-dependent heater temperature, we analyzed the sample temperature through simulation ('Simulation of the sample heating of upscaled sample' in Supplementary Note 4). We first considered two-dimensional scale-up, where the sample length and width are proportionally enlarged according to the heater dimensions, while maintaining the sample thickness. The temperature profiles of the sample follow the same pattern across different scales (Fig. 4c and Supplementary Fig. 10). The metric, time of T_{99}, representing the time required to heat the sample temperature to 99% of the heater temperature, remained independent of scale despite the exponential increase in sample mass (Fig. 4d). This underscores the excellent scalability of electrical heating for chlorination. The three-dimensional scale-up, where all three dimensions of the sample are proportionally enlarged, was also analyzed. In this case, time of T_{99} is increased with the sample size (Supplementary Figs. 11 and 12). Nevertheless, the temperature reached a plateau within ~1 min for the upscaled sample, still outperforming indirect heating methods that take hours to reach thermal balance.

Last, to experimentally demonstrate scalability, the ETC/ETCC for selective metal recovery was increased to gram scale, using a 2 inch (5.08 cm) tube reactor and a larger heater of 9×3 cm^2 (L/W). The reactor was first used for ETC recovery of In from ITO at gram scale (Extended Data Figs. 7a). Operating processes remained consistent with the small-scale reactions by using higher voltage inputs (Supplementary Table 3). Optimization resulted in a 98% purity and 91% yield of In (Extended Data Fig. 7b), comparable to small reactor results (Fig. 2f). A processing time of ~10 min equated to a productivity of 144 g per day from this laboratory reactor. Subsequently, we attempted to scale up the two-step ETC and ETCC process for selective recovery of Ta from TCW, also at gram scale (Fig. 4e and Extended Data Figs. 7c–h). We achieved 95.1% purity and 88.2% yield of Ta at the gram scale, mirroring the results obtained at the 50 mg scale. This suggested the potential for further scaling the electrothermal reactor. The above analysis and experiments validate the potential for scaling up the electrothermal reactor while mitigating secondary waste streams.

In our current experiments, we used chlorine gas as the chlorinating agent for the ETC/ETCC reaction. Unreacted chlorine can be easily recovered and recycled in an industrial implementation by condensation[32] or adsorption/desorption cycle[33]. While chlorine is often the preferred chlorinating agent on an industrial scale, other chlorinating agents such as chloride or waste chlorine-containing plastics such as polyvinyl chloride, can be used as the chlorinating agent[10]. Although we here demonstrated the selective recovery of one critical metal in e-waste, the ETC process is projected to be done in a continuous manner to selectively separate metals (Supplementary Fig. 13).

Technoeconomic and environmental considerations

In evaluating the economic feasibility, we conducted a technoeconomic analysis (TEA) to compare the capital costs (CAPEX) and operating costs (OPEX) of the ETC/ETCC process with currently deployed hydrometallurgical processes (Supplementary Note 5). Two generic ETC and ETCC processes were considered, encompassing process blocks such as Cl_2 introduction, ETC or ETCC reaction, gas recovery, off-gas treatment and post-treatment to obtain the metal oxide product (Extended Data Fig. 8 and Supplementary Data 2). As counterparts, two hydrometallurgical processes, acid leaching followed by solvent extraction[28,34] and alkaline digestion followed by selective leaching[35] (Extended Data Fig. 9 and Supplementary Data 2), were comparatively analyzed. CAPEX was estimated using scaling factors ranging from 1 to 100 tonnes per year. Monte Carlo simulations were implemented for sensitivity analyses. The results indicated a reduction in CAPEX with increased capacity (Fig. 4g), showcasing the economy of scale. The ETC and ETCC processes were expected to exhibit a 20–40% reduction in CAPEX compared with hydrometallurgical processes (Fig. 4g and Extended Data Fig. 10a). At a 1 tonne scale per year, the OPEX of the ETC and ETCC were ~$800 and ~$900, respectively (Fig. 4h and Extended Data Fig. 10b). In contrast, the acid leaching and alkaline digestion processes exhibited OPEX of ~$3,500 and ~$1,700, respectively. The OPEX of the electrothermal process represented 23–56% of the hydrometallurgical processes. The economic benefit of the ECT/ECTT can be ascribed to the compact reactor design and reduced operating procedures. While we primarily used a capacitor system to provide direct current input for joule heating, we showed that the alternating current is also applicable (Supplementary Fig. 14). This can further reduce the equipment cost of the ETC/ETCC process.

A cradle-to-gate life-cycle assessment (LCA) was conducted, aiming to examine the environmental impacts and energy demands of the ETC/ETCC process (Supplementary Note 6 and Supplementary Data 2). Acid leaching followed by solvent extraction, and alkaline digestion followed by selective leaching processes, served as representatives of hydrometallurgy for selective metal recovery. The functional unit was defined as the selective recovery of target metals from 1 tonne of mixed metal oxides. The global warming potential (GWP) of ETC and ETCC was estimated to be ~7.8 and ~8.8 tonnes, respectively, of CO_2 equivalent per tonne of feedstock (Fig. 4i and Extended Data Fig. 10c), which are 19–42% lower than that of the acid leaching (~13.4 tonnes) and alkaline digestion (~10.9 tonnes). The cumulative energy demand for ETC/ETCC processes was $\sim 5 \times 10^4$ MJ per tonne of feedstock, reflecting a 26–65% reduction compared with hydrometallurgical processes (Extended Data Fig. 10d). Notably, the ETC/ETCC process demonstrated substantially lower water resource depletion compared with the conventional acid leaching process (Extended Data Fig. 10e), owing to the minimal water consumption of the ETC/ETCC process. Considering that metal production constitutes a substantial part of global greenhouse gas emission[36], the ETC/ETCC process holds promise as a sustainable metal separations method for a low-carbon-footprint metal industry.

https://doi.org/10.1038/s44286-024-00125-2

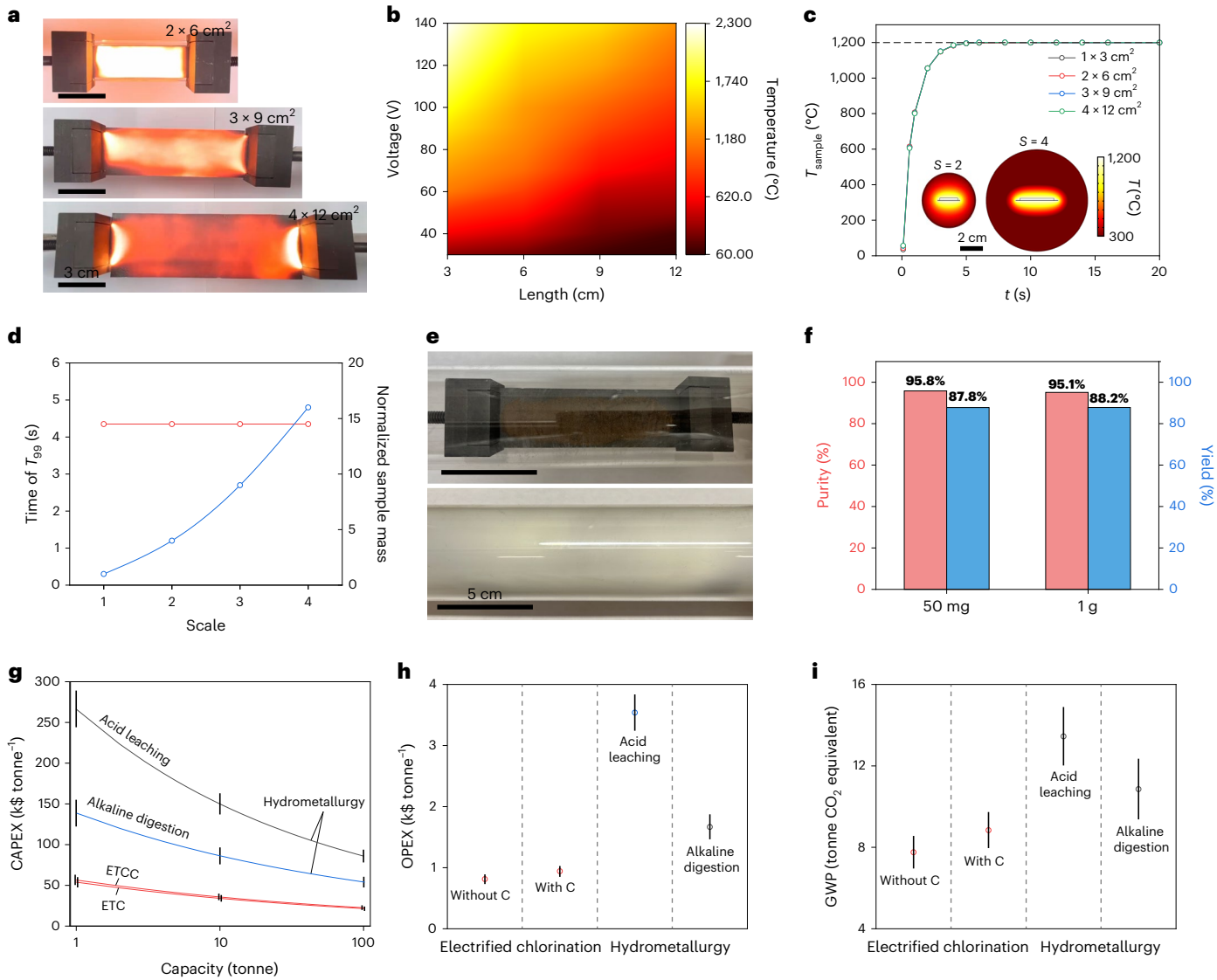

Fig. 4 | Scalability, technoeconomic and sustainability considerations. **a**, Pictures of carbon paper heaters under the same voltage input of 100 V, with sizes of 2 × 6 cm², 3 × 9 cm² and 4 × 12 cm² ($W \times L$). **b**, The heater temperature map versus voltage input and heater length. The thickness of the heater remains constant, and its aspect ratio (L/W) is fixed to 3. **c**, Simulated average temperature profile of sample with different heater scales (S). $S = 1$ represents 1 × 3 cm². The heater temperature is fixed to 1,200 °C. Inset: simulated temperature distribution for $S = 2$ and 4. **d**, Time of T_{99} and the normalized sample mass varied with heater scale. The sample mass is defined as 1 at the scale of 1. **e**, A picture of the raw TCW placed on the carbon heater with a size of 3 × 9 cm² (top) and the volatile deposited on the quartz tube after the second-step ETCC reaction (bottom). **f**, The purity and yield of the Ta product recovered from the scaled-up batch at 1.0 g. **g**, The capacity-dependent CAPEX of the separation of binary metal oxides using the ETC (with and without carbon) and the hydrometallurgical processes (acid leaching and alkaline digestion; k$, kilo dollars (United States dollars)). **h**, The OPEX of the separation of binary metal oxides using the ETC or the hydrometallurgical processes at capacity of 1 tonne. **i**, The GWP of the separation of binary metal oxides using the ETC or the hydrometallurgical processes at capacity of 1 tonne. The error bars in **g**–**i** denote one standard deviation, as determined through Monte Carlo uncertainty analysis from $N = 10^5$ iterations.

Discussion

The separation of In, Ga and Ta from their waste feedstocks represents three distinct patterns of the ETC/ETCC selectivity: (1) selective chlorination followed by evaporation that is based on the thermodynamic difference; (2) chlorination followed by selective evaporation that is based on boiling point differences; and (3) selective carbochlorination that is based on the kinetic differences. We compared the ETC/ETCC process with other indirect furnace heating-based chlorination processes for In, Ga and Ta recovery from e-wastes[20,23,24] (Supplementary Table 4). The ETC/ETCC process exhibits improvements regarding yield, purity and production rate. If the three metals were mixed together, they can be successfully separated as well (Supplementary Fig. 15).

Although we here primarily focused on the recovery of In, Ga and Ta as critical metals in electronics, 12 metals in total were involved in this process, including In, Sn, Mn, Au, Ta, Si, Fe, Ni, Cu, Ga, Ag and Cr. The high temperature of ETC extends the applicability of chlorination metallurgy. For example, using the ETC process, we show that the Cr_2O_3 can be converted to $CrCl_3$ at a temperature of >1,770 °C (Supplementary Fig. 16), which is beyond the temperature range of typical furnace heating. These metals involved in this work serve as good representatives to demonstrate the generality of our approach: In, Sn and Ga are *p*-block metals; Si is a metalloid; Mn, Ta, Fe, Ni, Cu and Cr are transition metals; and Au and Ag are precious metals within the transition metal block.

The incorporation of direct electric heating into the chlorination process represents a potential shift in metallurgy that could minimize supply chain shortage. The ability to achieve high temperatures greatly expands the applicability of metal feedstocks; the precise temperature control enhances metal separations based on subtle differences in chlorination free energies of formation; the rapid heating and cooling rates permit kinetic selectivity, allowing chlorination reactions with similar thermodynamics to be distinguished based upon rate differences; and the high energy efficiency of electric heating makes the metal recovery process more cost-effective. As a result, these performance improvements of ETC/ETCC processes greatly expand the potential generality, practicality and economic viability of chlorination metallurgy for metal recycling. While e-wastes were used in the current work, we envision that the process is applicable for industrial wastes such as coal fly ash[37] and bauxite residue[38], and even crude ores[19], considering that metal oxides constitute the majority of those feedstocks.

Methods

Materials

The chemicals used were In_2O_3 (MilliporeSigma, 99.998%), ITO (MilliporeSigma, −325 mesh, 99.99%), $InCl_3$ (MilliporeSigma, 98%), Ta_2O_5 (Sigma-Aldrich, 99%), SiO_2 powder and carbon black (Cabot, Black Pearls 2000). The carbon paper was purchased from FuelCellStore (Toray Carbon Paper 060). Carbon paper is chosen as the heater because it has appropriate resistance for joule heating, it is highly graphitized material that is stable up to 3,000 °C and it is also chlorine resistive (Supplementary Fig. 17). The TCF wastes for In recovery were purchased from eBay. The as-obtained TCF wastes were calcined at 800 °C in air for 2 h to remove the plastic substrate using a furnace (NEY 6-160A). The TCW for Ta recovery was purchased from eBay. The as-received TCW was calcined at 800 °C in air for 2 h to remove the plastic housings. The calcination step is required to remove the plastic so that the inorganic metal components are available for reaction with chlorine and to prevent extensive off-gassing during the electrothermal process. In practice, full-chain e-waste recycling involves an incineration step[39] to pyrolyze the organics and the thermal energy is recovered and used. Our process can follow analogously for the first step in the metal recovery. We here mimicked the LED manufacturing process to produce the wastes. Briefly, GaN (500 nm), Ag (500 nm), SiO_2 (500 nm) and Au (100 nm) layers were sequentially deposited on a prepatterned silicon wafer. After lift-off, the mixed metal powders were collected and dried using an oven at 120 °C for 2 h. The as-obtained dry mixed metal powder was used for the Ga recovery (Extended Data Fig. 5a).

Chlorine supply system

The scheme of the chlorine supply system is shown in Extended Data Fig. 1a. A Cl_2 cylinder (MilliporeSigma, 99.5%, 85 psi, 454 g) was used to supply the Cl_2. Argon gas (Airgas, 99.99%) combined with the pumping system was used to purge the system, which is essential to remove moisture and air before introducing Cl_2. The vacuum pump is made of stainless steel, and an ascarite halogen trap was affixed at the inlet of the pump to absorb most of the unreacted Cl_2. A reservoir is used between the Cl_2 cylinder and the gas pipelines, to provide limit Cl_2 release in case of cell failure. The CGA-180 fitting with polytetrafluoroethylene O-ring was used to connect the Cl_2 cylinder and the reservoir. The tubing and fitting of the chlorine supply system are made of stainless steel. The regulators and pressure gauges are made of Monel or stainless steel that are designed for corrosive gases. A needle valve combined with the rotameter was used to control the Cl_2 gas flow rate. A sodium hydroxide (NaOH) bath was used to absorb the unreacted Cl_2 gas. We note that, when industrialized, the unreacted Cl_2 can be easily recovered and reused.

Electrical system

The diagram of the electrical system to generate pulsed direct current is shown in Extended Data Fig. 1b,c. A capacitor bank that can reach voltage up to 500 V with a total capacitance of 0.624 F was used. The capacitor is charged by a d.c. supply. A variable-frequency drive was used to generate the pulse voltage with the frequency (f) ranging from 0 to 1,000 Hz, while in this work, f = 1,000 Hz was used. The duty cycle (or the on state period) is tunable, and in this work, a duty cycle of 5% or 10% was used. The current profile was recorded using a Multifunction I/O (NI USB-6009) controlled by LabView. The carbon paper was used as the heater, which was secured on a graphite block and then connected to electrical system through two graphite electrodes that are inert to Cl_2. For the carbon paper with size of 1 × 3 cm^2, the resistance is ~0.7 Ω, which is appropriate for the joule heating. We note that an appropriate resistance is critical for effective heating (see 'Discussion' in Supplementary Note 4).

ETC and ETCC reactor and process

In a typical small-scale experiment, a carbon paper size of 1 × 3 cm^2 was used for a sample mass of 100 mg. The sample was loaded on the carbon paper heater, which was connected to the capacitor bank. The sample was put into a sealed quartz tube. After purging the system three times, Cl_2 was introduced at a flow rate of ~20 sccm for the small-scale sample and ~40 sccm for the large-scale sample. The pulse current input brings the carbon paper heater to a desired temperature. The sample and gas temperatures rapidly follow the pattern of heater temperature, as shown in Fig. 1g. The volatiles were deposited on the quartz tube. The chloride product is usually deliquescent, so the sample sealed in the quartz tube was transferred into a glove box, and the sample was then collected by scarping with a spatula from the quartz wall; the chlorides were loosely deposited on the inner quartz tube. The residue remaining on the carbon paper is also easily collected. In other cases, the sample was oxidized in air to isolate the pure metal oxide. The detailed experimental conditions for each experiment are presented in Supplementary Table 3. For Ta recovery from TCW, after the first-step ETC process, most of the metal chloride impurities were evaporatively removed from the residual Ta_2O_5 and SiO_2. In addition, a water rinsing step can be used to further remove the metal chloride impurities.

Temperature measurement

Temperatures below 200 °C were measured using an infrared thermometer (KIZEN LaserPro LP300). Temperatures between 200 and 1,500 °C were measured using a thermometer (Micro-Epsilon, CTM-3SF75H2-C3). Temperatures between 1,500 and 3,000 °C were measured using a thermometer (Micro-Epsilon, CTRM-1H1SF100-C3). Both thermometers have a time resolution of 1 ms. Due to the available temperature range, different thermometers were used for the temperature measurement at voltage input of 30–60 V and 80–140 V, which leads to the discontinuity of the temperature–voltage curves (Fig. 1f).

Characterization

Raman spectra were acquired using a Renishaw Raman microscope (laser wavelength of 532 nm, laser power of 5 mW, 50× lens). SEM images were obtained using a FEI Quanta 400 ESEM FEG system at 20 kV. EDS spectra and maps were acquired using the same system equipped with an EDS detector. X-ray photoelectron spectroscopy (XPS) was conducted using a PHI Quantera XPS system at a base pressure of 5×10^{-9} Torr. Elemental spectra were obtained with a step size of 0.1 eV with a pass energy of 26 eV. All the XPS spectra were calibrated using the standard C 1s peak at 284.8 eV. XRD was acquired using a Rigaku Smartlab II system configured with a Cu Kα radiation (λ = 1.5406 Å). Since $InCl_3$ is very deliquescent, we used Kapton tape to seal the $InCl_3$, avoiding contacting moisture during the XRD measurement. The broad peak at 26.3° in the XRD pattern (Fig. 2e) was ascribed to the tape substrate.

Sample digestion and ICP-MS measurement

The samples were digested using acid and the metal contents were measured using ICP-MS. HNO_3 (67–70 wt%, trace metal grade, Fisher

Chemical), HCl (37 wt%, 99.99%, trace metal basis, MilliporeSigma), HF (48 wt%, 99.99%, trace metal grade for ICP analysis, MilliporeSigma) and ultrapure water (MilliporeSigma, American Chemical Society (ACS) reagent for ultratrace analysis) were used for sample digestion. The ITO or the TCF waste samples were digested using an aqua regia method. Specifically, 50 mg of ITO or the TCF waste was dissolved using 3 ml of concentrated HCl and 1 ml of concentrated HNO_3 at 90 °C for 2 h. Then, the solution was diluted to target concentrations using ultrapure water. In the recovery of In from ITO and the TCF wastes, the volatile was dissolved using 2 wt% HCl, while the residue was digested using the aforementioned aqua regia process. For the recovery of Ga from LED manufacturing wastes, the raw wastes and the residue after the ETC process were digested using the aforementioned aqua regia process, and the volatile fraction was dissolved using 2 wt% HCl. For the recovery of Ta from TCW, all samples, including the TCW raw materials as well as the volatiles and the residues in both the first-step ETC and the second-step ETCC reactions, were digested using a HF:HCl:HNO_3 process. HF was required to dissolve the silicon in these samples[40]. Specifically, 50 mg of the sample was dissolved in the mixed acid of 3 ml HCl, 1 ml HNO_3 and 1 ml HF. Then, the solution was filtered using a sand core funnel (class F) and diluted to target concentrations using ultrapure water.

ICP-MS was conducted to measure the metal contents, using a PerkinElmer Nexion 300 ICP-MS system. The below standards were used: Periodic Table mix 1 (MilliporeSigma, 33 elements of Al, As, Ba, Be, Bi, B, Ca, Cd, Cs, Cr, Co, Cu, Ga, In, Fe, Pb, Li, Mg, Mn, Ni, P, K, Rb, Se, Si, Ag, Na, Sr, S, Te, Tl, V and Zn, 10 mg l^{-1} each, in 10 wt% HNO_3 containing HF traces), Periodic Table mix 2 (MilliporeSigma, 17 elements of Au, Ge, Hf, Ir, Mo, Nb, Pd, Pt, Re, Rh, Ru, Sb, Sn, Ta, Ti, W and Zr, 10 mg l^{-1} each, in 5% HF and 1% HCl containing HNO_3 traces), individual standard of In, Sn, Y, Ta, Ni, Fe, Ta, Cu and Mn (MilliporeSigma, 1,000 mg l^{-1} in 2% HNO_3) and Si (Agilent Technologies, 1,000 g l^{-1} in water with dilute HNO_3 and HF acid). For the total quantification of metal contents in wastes, including TCF and TCW, the mixture standards were used. For the In recovery from ITO, In and Sn standards were used with Y as the inner standard. For the In recovery from TCF wastes, Cr, Au, In, Sn and Mn standards were used with Y as the inner standard. For the Ga recovery from LED manufacturing wastes, Au, Ag, Ga and Si standards were used with Y as the inner standard. For the Ta recovery from TCW, Ta, Si, Cu, Fe, Ni and Mn standards were used with Y as the inner standard. All samples were measured in triplicate to afford the standard deviations.

TEA

Four scenarios were considered in the TEA: (1) the ETC process, including the following processing blocks: N_2 introduction for purging and its recovery for reuse, Cl_2 introduction for chlorination, chlorination of mixed oxide feedstocks using an electrothermal reactor, off-gas (O_2 and unreacted Cl_2) separation using a distillation column and the recovery of Cl_2, calcination of chloride to convert it to oxide using a rotary kiln, and an acid plant to capture the HCl off-gas and production of the hydrochloric acid by-product; (2) the ETCC process, including the following processing blocks: N_2 introduction for purging and its recovery for reuse, Cl_2 introduction for chlorination, carbon introduction for reaction, carbon chlorination of mixed feedstocks using an electrothermal reactor, off-gas (CO and unreacted Cl_2) separation using a distillation column and the recovery of Cl_2, the combustion of CO off-gas using a combustor, rotary kiln for chloride calcination, and acid plant for HCl capture and hydrochloric acid production; (3) the acid leaching–solvent extraction process, including the following blocks: acid leaching of mixed metal feedstocks, solvent extraction for metal separation, stripping for metal recovery in aqueous phase, precipitation of metal, filtration, calcination to obtain the metal oxide, acid and extractant recovery, and wastewater and acid waste treatment; (4) the alkaline digestion–selective leaching process, including the following blocks: alkaline calcination of mixed oxide feedstocks, acid leaching of the calcined materials, filtration, secondary acid leaching of the residue, filtration to obtain the metal oxide product, gas recovery, and wastewater and acid waste treatment.

The global production rates of the critical metals considered in this work (In, Ga and Ta) are on the order of 1,000 tonnes per year. Hence, we here considered three feed capacities ranging from 1 to 100 metric tonnes per year. For the CAPEX estimation, we considered the inside battery limits, while outside battery limits and engineering and construction costs were not considered. As a preliminary estimate or 'class 4' estimate, we used an accuracy of ±30% according to the Association for the Advancement of Cost Estimating International. A detailed description of equipment, materials flows, processing parameters, energy consumption and materials and energy expense inventory is shown in Supplementary Note 5. The sensitivity analysis was conducted via Monte Carlo simulation. The code used for the Monte Carlo simulation was written by the authors and is provided with this paper. Total equipment preexponential, operating parameters, materials consumptions, materials costs and process costs, all with a class 4 error (±30%), were each randomly varied using continuous triangular distributions for the simulation.

LCA

The environmental impact is evaluated via LCA (Supplementary Note 6). The same four scenarios (that is, ETC process, ETCC process, acid leaching–solvent extraction and alkaline digestion–selective leaching) used in the TEA study were considered here (Extended Data Figs. 8 and 9). The functional unit of this study is the metal separation from 1 tonne of mixed metal oxide feedstock. The system boundary is defined to be the input of mixed metal oxide and the output of separated metal oxides. Life-cycle inventory (LCI) data (Supplementary Data 2.7) for inputs are from Argonne National Laboratory GREET Model[41] and ecoinvent 3.8 global averages[42]; if not available in these databases, the LCI data were cited from representative literatures. The LCI entries were converted into environmental impacts using the ReCiPe 2016 methodology[43]. Three environmental impacts were considered in this work, including GWP in 100 years (GWP 100a), cumulative energy demand and water resource depletion. Monte Carlo simulation was conducted for the sensitivity analysis. The code used for the Monte Carlo simulation was written by the authors and is provided with this paper. Briefly, 10^5 iterations were conducted over the process parameters including materials consumptions and process energy consumption, which are varied using continuous triangular distributions. The upper and lower limits for the triangular distribution were taken as +30% and −30% of the base values.

Data availability

The data supporting the findings of the study are available within the Article and its Supplementary Information. Source data generated in this study are uploaded to the Zenodo repository at https://doi.org/10.5281/zenodo.13331446 (ref. 44). Source data are provided with this paper.

Code availability

Source code and its description file for TEA and LCA are provided with this paper.

References

1. Reck, B. K. & Graedel, T. E. Challenges in metal recycling. *Science* **337**, 690–695 (2012).
2. Sovacool, B. K. et al. Sustainable minerals and metals for a low-carbon future. *Science* **367**, 30–33 (2020).
3. Watari, T., Nansai, K. & Nakajima, K. Review of critical metal dynamics to 2050 for 48 elements. *Resour. Conserv. Recycl.* **155**, 104669 (2020).

4. Frenzel, M., Mikolajczak, C., Reuter, M. A. & Gutzmer, J. Quantifying the relative availability of high-tech by-product metals—the cases of gallium, germanium and indium. *Resour. Policy* **52**, 327–335 (2017).
5. Frenzel, M., Ketris, M. P., Seifert, T. & Gutzmer, J. On the current and future availability of gallium. *Resour. Policy* **47**, 38–50 (2016).
6. Matsuoka, R., Mineta, K. & Okabe, T. H. Recycling process for tantalum and some other metal scraps. *Proc. TMS Fall Extr. Process. Conf.* **2004**, 689–696 (2004).
7. Martelo, L. M., Sousa, P. M. S., Silva, M. A. D. & Soares, H. M. V. M. A critical updated review of all stages of the tantalum recycling chain from waste of tantalum capacitors. *Chem. Eng. J.* **472**, 144917 (2023).
8. *U.S. Department of Energy's Strategy to Support Domestic Critical Mineral and Material Supply Chains (FY 2021–FY 2031)* (U.S. Department of Energy, 2021).
9. Ghosh, B., Ghosh, M. K., Parhi, P., Mukherjee, P. S. & Mishra, B. K. Waste printed circuit boards recycling: an extensive assessment of current status. *J. Clean. Prod.* **94**, 5–19 (2015).
10. Deng, B. et al. Urban mining by flash joule heating. *Nat. Commun.* **12**, 5794 (2021).
11. Ogunseitan, O. A., Schoenung, J. M., Saphores, J.-D. M. & Shapiro, A. A. The electronics revolution: from e-wonderland to e-wasteland. *Science* **326**, 670–671 (2009).
12. Olivetti, E. A. & Cullen, J. M. Toward a sustainable materials system. *Science* **360**, 1396–1398 (2018).
13. Raabe, D., Tasan, C. C. & Olivetti, E. A. Strategies for improving the sustainability of structural metals. *Nature* **575**, 64–74 (2019).
14. Sun, Z. et al. Toward sustainability for recovery of critical metals from electronic waste: the hydrochemistry processes. *ACS Sustain. Chem. Eng.* **5**, 21–40 (2017).
15. Jadhav, U. & Hocheng, H. Hydrometallurgical recovery of metals from large printed circuit board pieces. *Sci. Rep.* **5**, 14574 (2015).
16. Lu, X. et al. A solid-state electrolysis process for upcycling aluminium scrap. *Nature* **606**, 511–515 (2022).
17. Stinn, C. & Allanore, A. Selective sulfidation of metal compounds. *Nature* **602**, 78–83 (2022).
18. Jena, P. K. & Brocchi, E. A. Metal extraction through chlorine metallurgy. *Miner. Process. Extr. Metall. Rev.* **16**, 211–237 (1997).
19. Xing, Z., Cheng, G., Yang, H., Xue, X. & Jiang, P. Mechanism and application of the ore with chlorination treatment: a review. *Miner. Eng.* **154**, 106404 (2020).
20. Niu, B., Chen, Z. & Xu, Z. Method for recycling tantalum from waste tantalum capacitors by chloride metallurgy. *ACS Sustain. Chem. Eng.* **5**, 1376–1381 (2017).
21. Niu, L.-P., Zhang, T.-A., Ni, P.-Y., LÜ, G.-Z. & Ouyang, K. Fluidized-bed chlorination thermodynamics and kinetics of Kenya natural rutile ore. *Trans. Nonferrous Met. Soc. China* **23**, 3448–3455 (2013).
22. Glaeser, H. H. & Spoon, M. J. Fluidized bed process for chlorinating titanium-containing material and coke useful in such process. U.S. patent US5389353A (1988).
23. Terakado, O., Saeki, T., Irizato, R. & Hirasawa, M. Pyrometallurgical recovery of indium from dental metal recycling sludge by chlorination treatment with ammonium chloride. *Mater. Trans.* **51**, 1136–1140 (2010).
24. Gustafsson, A. M. K., Steenari, B.-M. & Ekberg, C. Recycling of CIGS solar cell waste materials: separation of copper, indium, and gallium by high-temperature chlorination reaction with ammonium chloride. *Sep. Sci. Technol.* **50**, 2415–2425 (2015).
25. Chen, Y. et al. Ultra-fast self-assembly and stabilization of reactive nanoparticles in reduced graphene oxide films. *Nat. Commun.* **7**, 12332 (2016).
26. Yao, Y. et al. Carbothermal shock synthesis of high-entropy-alloy nanoparticles. *Science* **359**, 1489–1494 (2018).
27. Luong, D. X. et al. Gram-scale bottom-up flash graphene synthesis. *Nature* **577**, 647–651 (2020).
28. Virolainen, S., Ibana, D. & Paatero, E. Recovery of indium from indium tin oxide by solvent extraction. *Hydrometallurgy* **107**, 56–61 (2011).
29. Angerer, T., Luidold, S. & Antrekowitsch, H. Recycling potentials of the two refractory metals tantalum and niobium. In *Proc. EMC* 1069–1084 (GDMB, 2013).
30. Niu, B., Chen, Z. & Xu, Z. Recovery of tantalum from waste tantalum capacitors by supercritical water treatment. *ACS Sustain. Chem. Eng.* **5**, 4421–4428 (2017).
31. Chiera, N. M. et al. Formation and thermochemical properties of oxychlorides of niobium (Nb) and tantalum (Ta): towards the gas-phase investigation of dubnium (Db) oxychloride. *Inorganica Chim. Acta* **486**, 361–366 (2019).
32. Sutter, R. C. Recovery of chlorine from air–chlorine mixtures. *J. Air Pollut. Control Assoc.* **7**, 30–31 (1957).
33. Watzenberger O., Pfeffinge J. Selective separation and recovery of chlorine from gas mixtures. US5788743A (1996).
34. Koleini, S. M. J., Mehrpouya, H., Saberyan, K. & Abdolahi, M. Extraction of indium from zinc plant residues. *Miner. Eng.* **23**, 51–53 (2010).
35. Xia, L., Wei, X., Wang, H., Ye, F. & Liu, Z. Valuable metal recovery from waste tantalum capacitors via cryogenic crushing-alkaline calcination-leaching process. *J. Mater. Res. Technol.* **16**, 1637–1646 (2022).
36. Yokoi, R., Watari, T. & Motoshita, M. Future greenhouse gas emissions from metal production: gaps and opportunities towards climate goals. *Energy Environ. Sci.* **15**, 146–157 (2022).
37. Deng, B. et al. Rare earth elements from waste. *Sci. Adv.* **8**, eabm3132 (2022).
38. Jovičević-Klug, M., Souza Filho, I. R., Springer, H., Adam, C. & Raabe, D. Green steel from red mud through climate-neutral hydrogen plasma reduction. *Nature* **625**, 703–709 (2024).
39. Stewart, E. S. & Lemieux, P. M. Emissions from the incineration of electronics industry waste. In *IEEE International Symposium on Electronics and the Environment* 271–275 (IEEE, 2003).
40. Xu, J., Guo, Y., Yang, S., Hohl, S. V. & Zhang, W. Reliable determination of SiO_2 concentrations in sediments via sequential leaching and ICP-OES/MS analysis. *J. Geochem. Explor.* **242**, 107090 (2022).
41. Argonne GREET model. *Argonne National Laboratory* https://greet.anl.gov/databases (accessed 11 September 2024).
42. Ecoinvent-Association ecoinvent 3.8. *Ecoinvent* https://ecoinvent.org/the-ecoinvent-database/ (accessed 11 September 2024).
43. Huijbregts, M. A. J. et al. ReCiPe2016: a harmonised life cycle impact assessment method at midpoint and endpoint level. *Int. J. Life Cycle Assess.* **22**, 138–147 (2017).
44. Deng, B. Flash separation of metals. *Zenodo* https://doi.org/10.5281/zenodo.13331446 (2024).

Acknowledgements

We thank H. Gonnermann of Rice University for allowing us to use the FEM simulation software, B. Chen of Rice University for helpful input with the XPS results and C. Pennington for developing and ICP-MS methods. We thank Z. Li, H. Zhao and J. Tian for helpful discussion on the LCA and TEA. The funding of the research was provided by the Defense Advanced Research Projects Agency (HR00112290122, J.M.T.), the US Army Corps of Engineers, ERDC (W912HZ-21-2-0050, J.M.T.), the Rice Academy Fellowship (Y.C.) and the startup funds of THU (B.D.).

Author contributions

B.D. conceived the idea and conducted the thermodynamic analyses. B.D., S.X. and C.K. built the chlorination equipment. B.D. and S.X. conducted the experiment with the help of J. Shin, Y.C., K.J., J. Sharp, L.Q. and S.C. L.E. built and maintained the electrical system. B.D. conducted

the numeric simulation. B.D. conducted the TEA and LCA and analyzed the results. B.D., S.X. and J.M.T. wrote the manuscript. All aspects of the research were overseen by J.M.T. All authors have discussed the results and given approval to the final version of the manuscript.

Competing interests

A PCT patent application has been filed on the ETC and ETCC process for selective metal recovery from electronic wastes and ores (PCT/US2023/076707). The patent applicant is Rice University, and the inventors are J.M.T., B.D. and C.K. This application has been licensed to a company in which J.M.T. is a stockholder, but he is not an officer, director or employee. Conflicts are mitigated through regular disclosure to and compliance with the Rice University Office of Research Integrity. The other authors declare no other competing interests.

Additional information

Extended data is available for this paper at https://doi.org/10.1038/s44286-024-00125-2.

Supplementary information The online version contains supplementary material available at https://doi.org/10.1038/s44286-024-00125-2.

Correspondence and requests for materials should be addressed to Bing Deng or James M. Tour.

Peer review information *Nature Chemical Engineering* thanks Xiangdong Zhu and the other, anonymous, reviewer(s) for their contribution to the peer review of this work.

https://doi.org/10.1038/s44286-024-00125-2

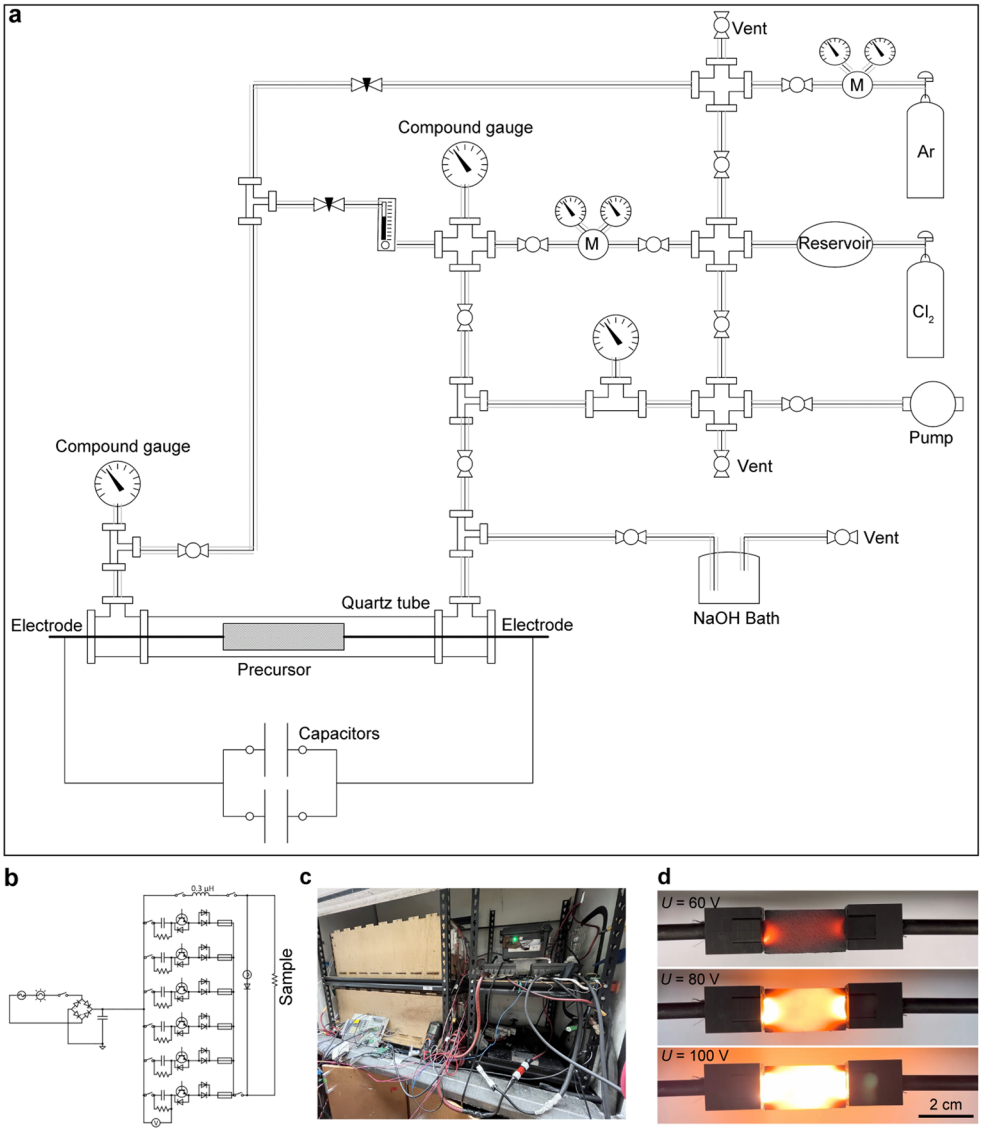

Extended Data Fig. 1 | Electrothermal chlorination system. (**a**) Scheme of the electrothermal chlorination system. (**b**) Electric diagram of the electric system. (**c**) Photograph of the electric system. (**d**) Photographs of the carbon heater under different voltage input ranging from 60 V to 100 V.

https://doi.org/10.1038/s44286-024-00125-2

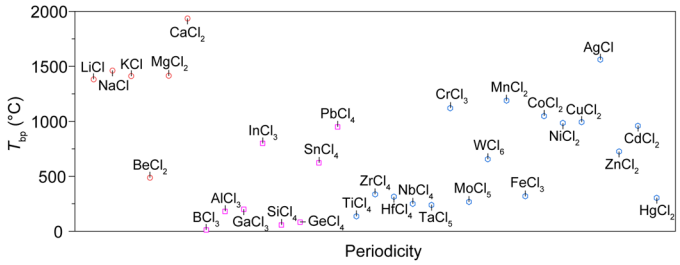

Extended Data Fig. 2 | Boiling points of metal chlorides.

https://doi.org/10.1038/s44286-024-00125-2

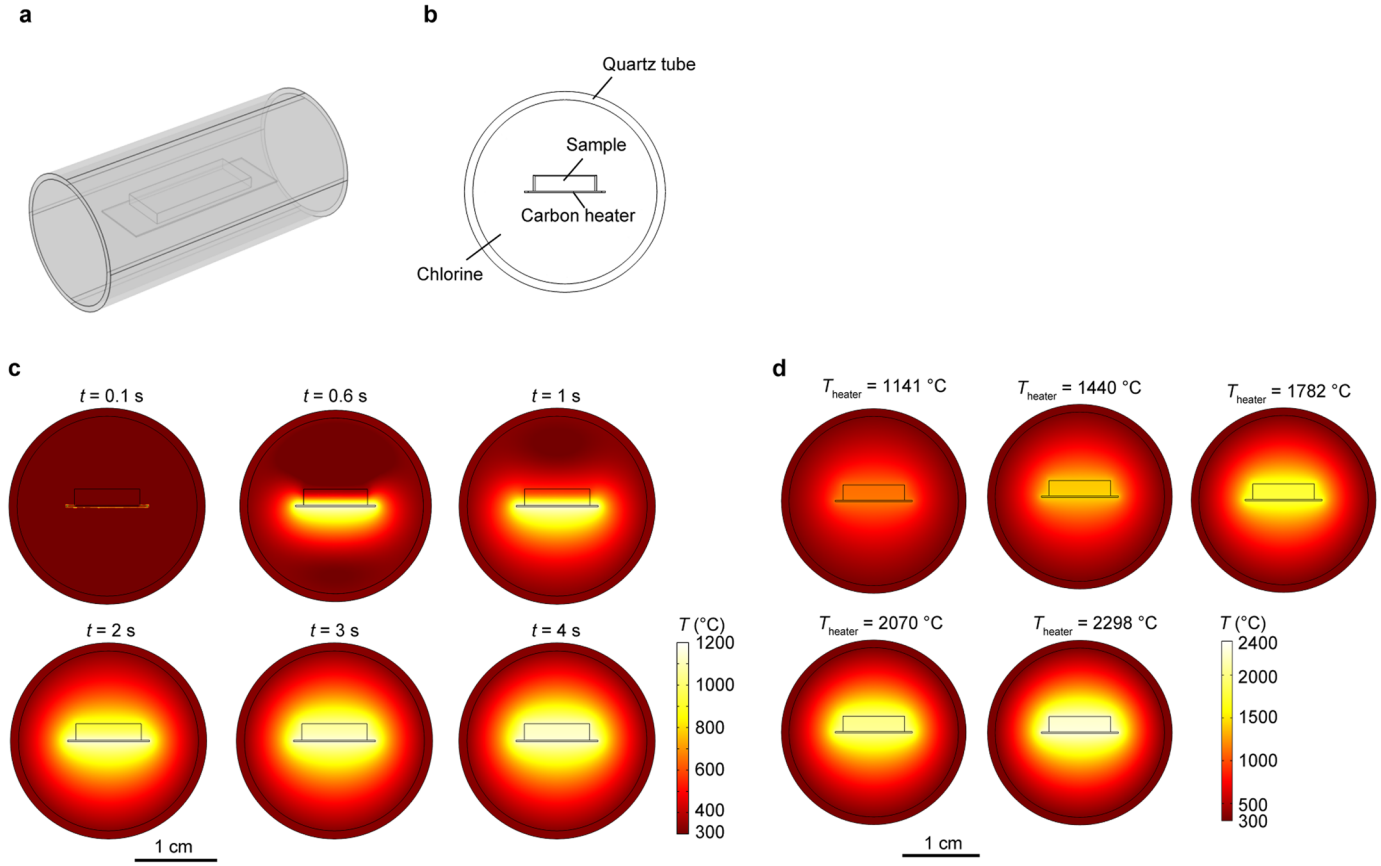

Extended Data Fig. 3 | Heat transfer simulation. (**a**) 3D framework of the simulation configuration. (**b**) Cross-section geometry of the simulation. (**c**) Simulated temperature distribution at different heating time, ranging from 0.1 s to 4 s. (**d**) Simulated temperature distribution at $t = 4$ s under different carbon heater temperatures (T_{heater}).

https://doi.org/10.1038/s44286-024-00125-2

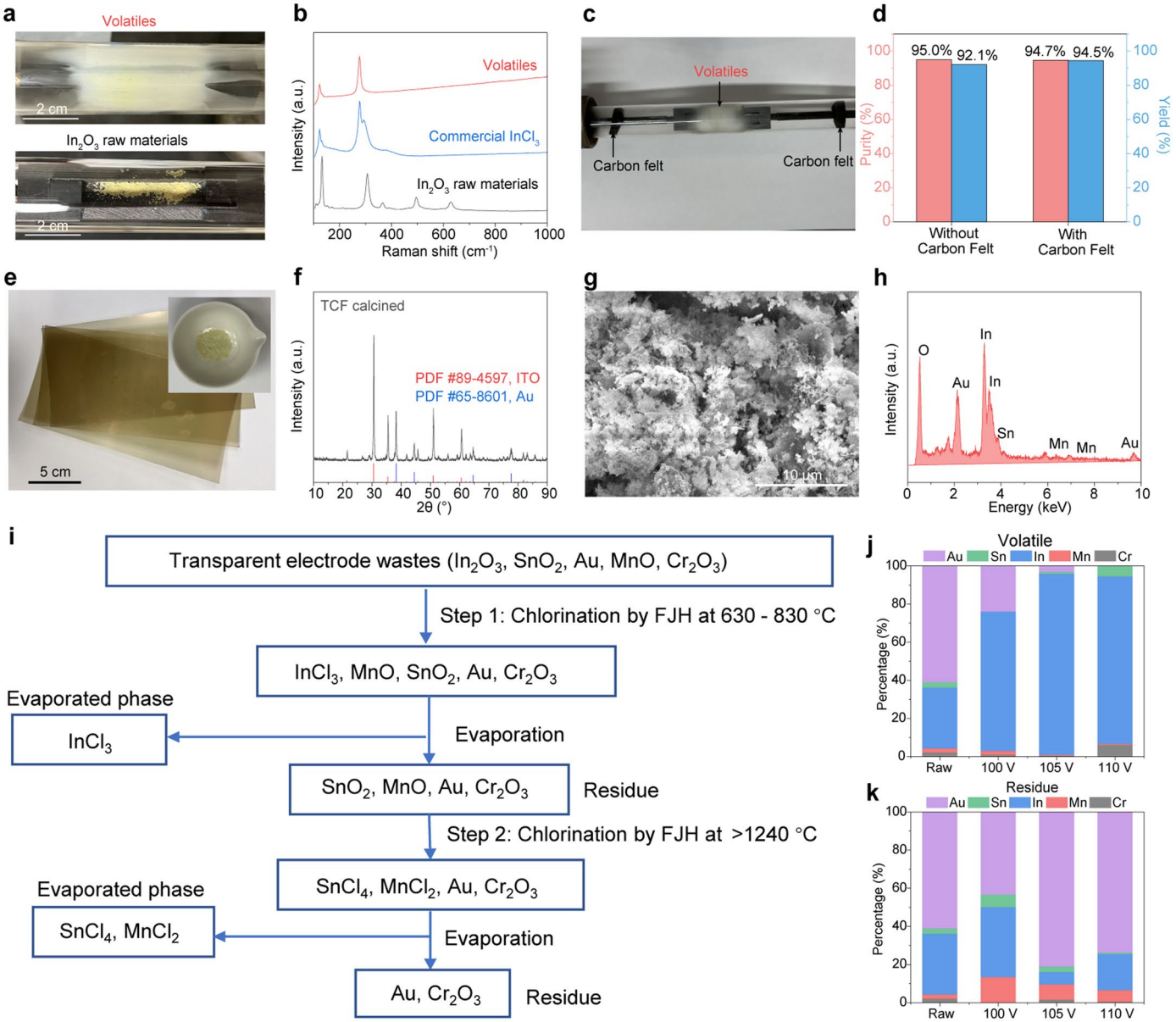

Extended Data Fig. 4 | In recovery from ITO waste. (**a**) Pictures of the In_2O_3 raw materials placed on the heater (bottom) and the $InCl_3$ volatiles deposited on the quartz tube. (**b**) Raman spectra of the In_2O_3 raw materials, commercial $InCl_3$, and the as-obtained $InCl_3$ volatiles. (**c**) Photographs of ITO raw materials (top) and the volatile deposited on quartz tube after chlorination (bottom). (**d**) Purity and yield of In when chlorinating ITO waste with or without porous carbon felt blocking the quartz tube. (**e**) Picture of the TCF. Inset, picture of the powder after removing the plastic substrate by calcination in air for 2 h at 800 °C. (**f**) XRD pattern of the powder after removing the plastic substrates by calcination. (**g**) SEM image of the powder. (**h**) EDS spectrum of the powder. (**i**) Protocol for the separation of In from the TCF waste powder. (**j**) Elemental composition of the raw materials and the volatile under different voltage input. (**k**) Elemental composition of the raw materials and the residue under different voltage input.

https://doi.org/10.1038/s44286-024-00125-2

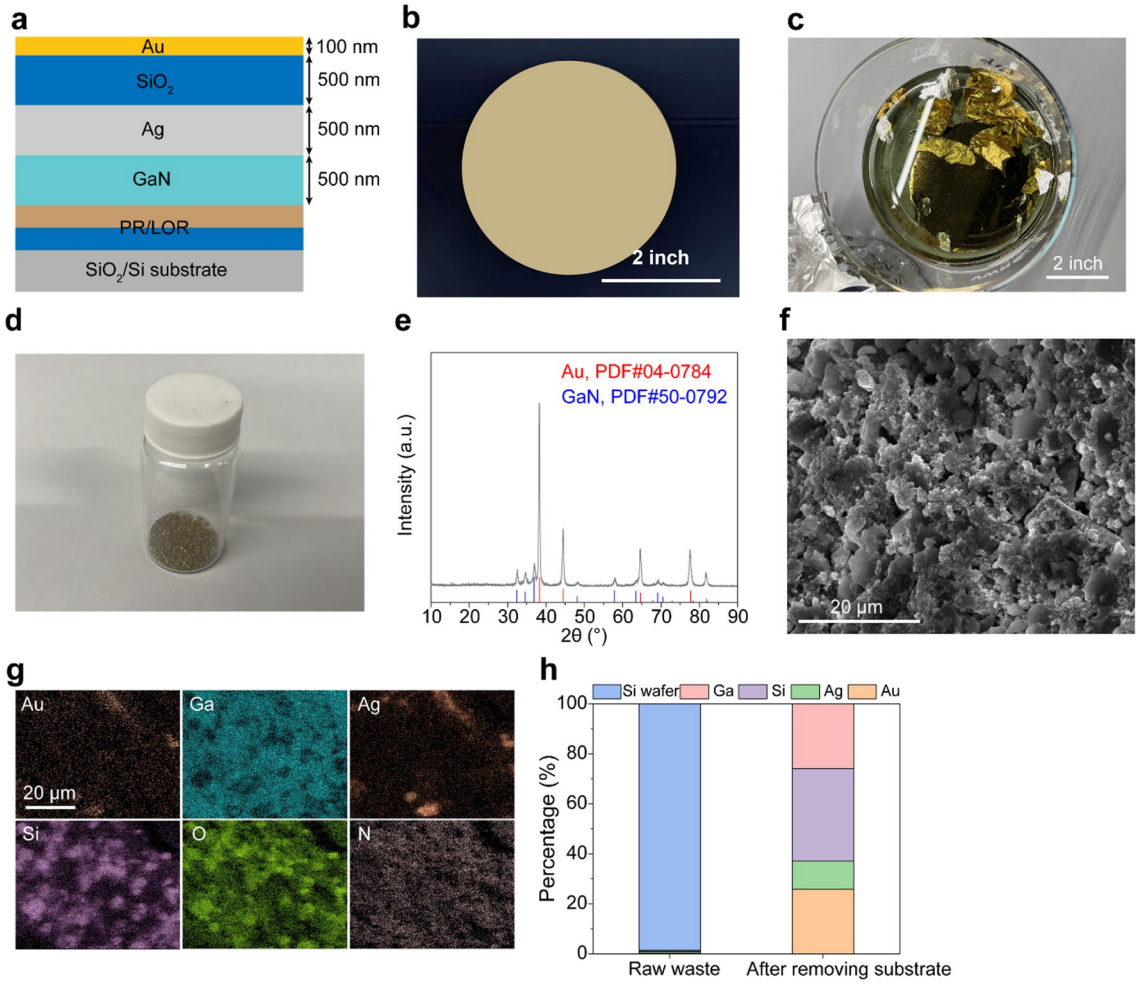

Extended Data Fig. 5 | Characterization of LED manufacturing wastes. (**a**) Schematic of the sputtering layers. (**b**) Picture of the silicon wafer with sputtered layers. (**c**) Picture of the lift-off process. (**d**) Picture of the mixed metal power after removing the Si substrates by lift-off. (**e**) XRD patterns. (**f**) SEM image. (**g**) Elemental maps. (**h**) Elemental composition of the raw wastes with Si substrates and the waste after removing substrates.

https://doi.org/10.1038/s44286-024-00125-2

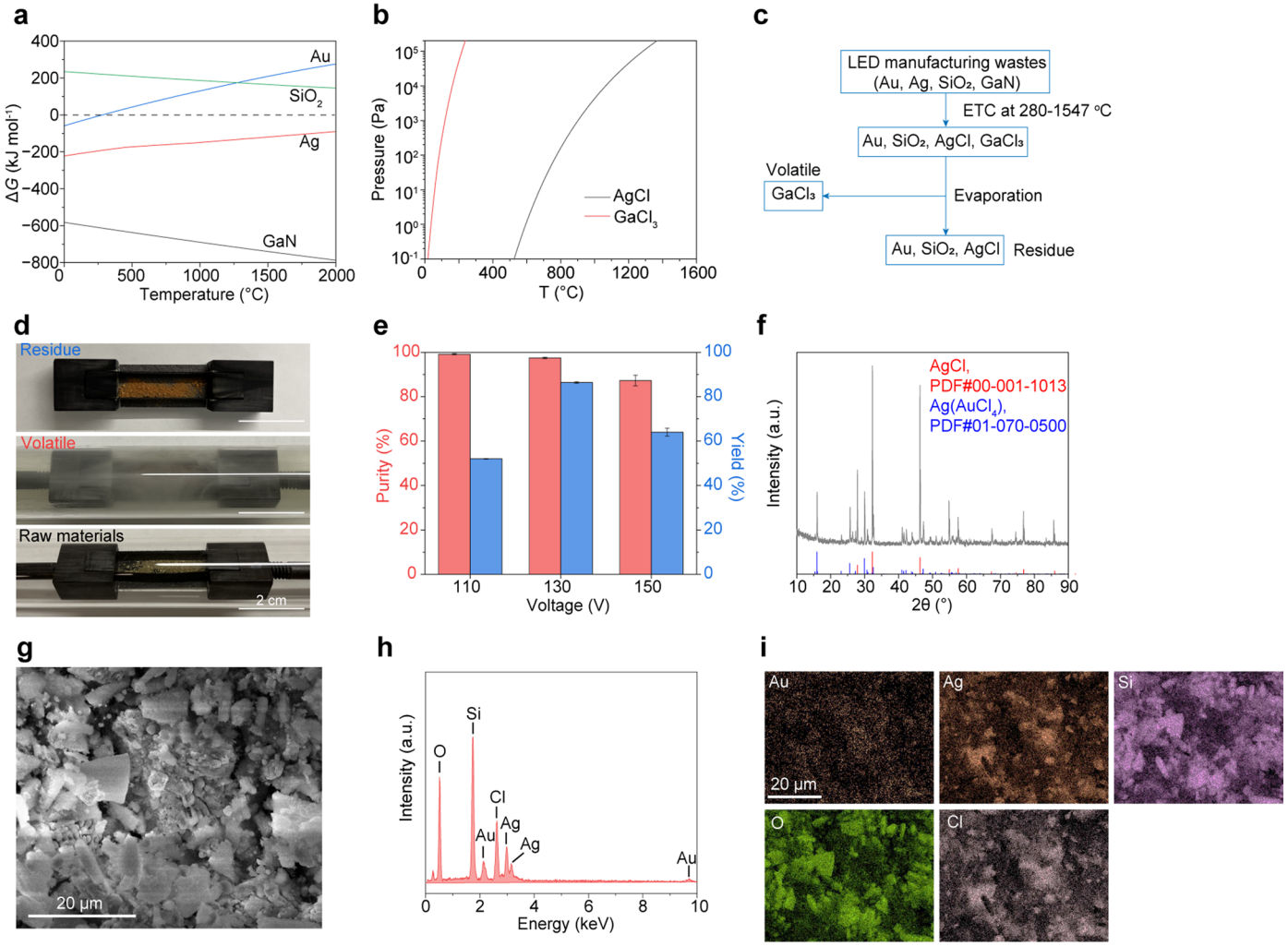

Extended Data Fig. 6 | Recovery of Ga from LED manufacturing wastes. (**a**) Thermodynamical analysis of the chlorination of metals in the LED manufacturing wastes. (**b**) Vapor pressure curves of AgCl and $GaCl_3$. (**c**) Protocol for the selective recovery of Ga from LED manufacturing waste. (**d**) Pictures of the electrothermal chlorination process. Bottom, raw materials; middle, the volatiles deposited on the quartz tube; top, the residue on the carbon paper heater. (**e**) Purity and yield of the Ga recovery from the LED manufacturing wastes varied with voltage input. (**f**) XRD pattern of the residue. (**g**) SEM image of the residue. (**h**) EDS spectrum of the residue. (**i**) EDS maps of the residue.

https://doi.org/10.1038/s44286-024-00125-2

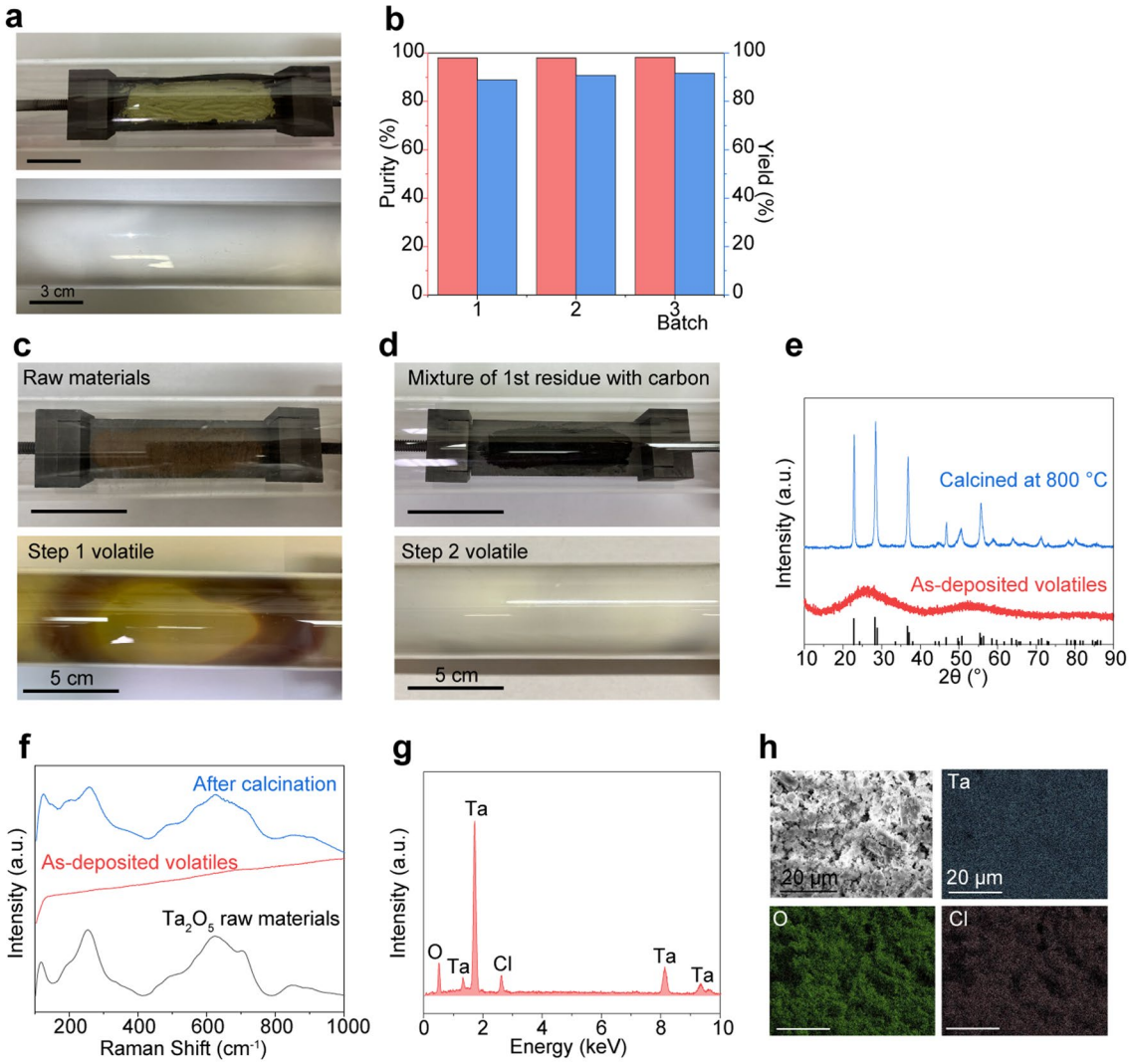

Extended Data Fig. 7 | Scaling up of the ETC/ETCC process. (**a**) Pictures of the ITO raw materials of 1.0 g (top) and the volatile deposited on the quartz tube (bottom) at 1.0 g scale. (**b**) Purity and yield of In product at different batches. (**c**) Pictures of the TCW raw materials of 1.0 g (top), and the volatile deposited on quartz tube obtained in the first-step ETC process (bottom). (**d**) Pictures of the mixture of the first-step residue and C (top), and the volatiles deposited on quartz tube obtained in the second-step ETCC process (bottom). (**e**) XRD patterns of the second-step as-deposited volatile and that after calcination. (**f**) Raman spectra of the second-step as-deposited volatile and that after calcination. (**g**) EDS spectrum of the second-step as-deposited volatiles. (**h**) SEM image and EDS elemental maps of the volatiles.

https://doi.org/10.1038/s44286-024-00125-2

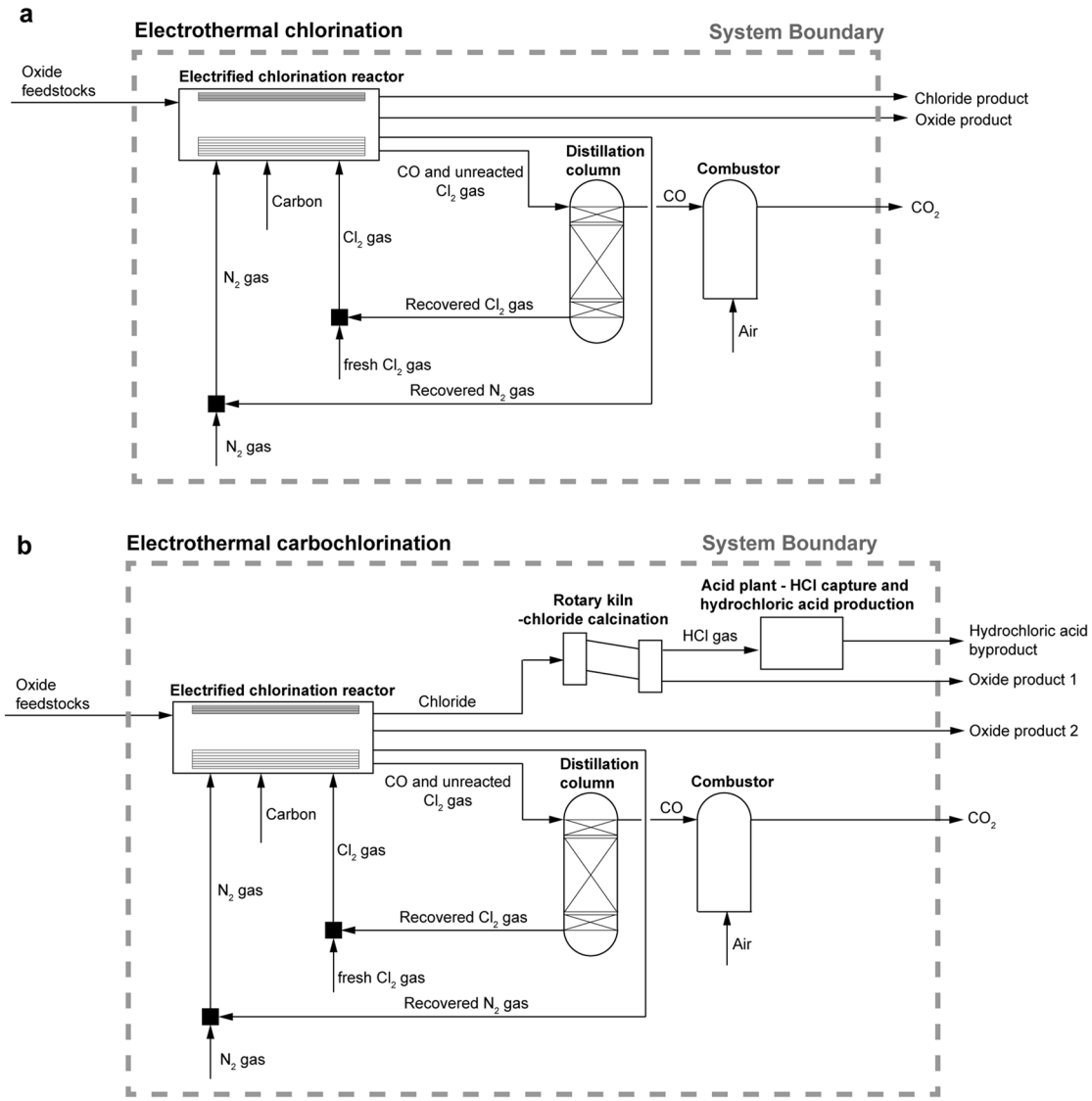

Extended Data Fig. 8 | Flowsheet of electrothermal chlorination and electrothermal carbochlorination. (**a**) Electrothermal chlorination with posttreatment to produce oxide product. This process includes N_2 introduction for purging and its recovery for reuse, Cl_2 introduction for chlorination, chlorination of mixed oxide feedstocks using an electrothermal reactor, off-gas (O_2 and unreacted Cl_2) separation using a distillation column and the recovery of Cl_2, calcination of chloride to convert it to oxide using rotary kiln, and an acid plant to capture the HCl off-gas and production of the hydrochloric acid by-product. (**b**) Electrothermal carbochlorination with posttreatment to produce oxide product. This process includes N_2 introduction for purging and its recovery for reuse, Cl_2 introduction for chlorination, carbon introduction for reaction, carbochlorination of mixed feedstocks using an electrothermal reactor, off-gas (CO and unreacted Cl_2) separation using a distillation column and the recovery of Cl_2, the combustion of CO off-gas using a combustor, calcination of chloride to convert it to oxide using rotary kiln, and an acid plant to capture the HCl off-gas and production of the hydrochloric acid by-product.

https://doi.org/10.1038/s44286-024-00125-2

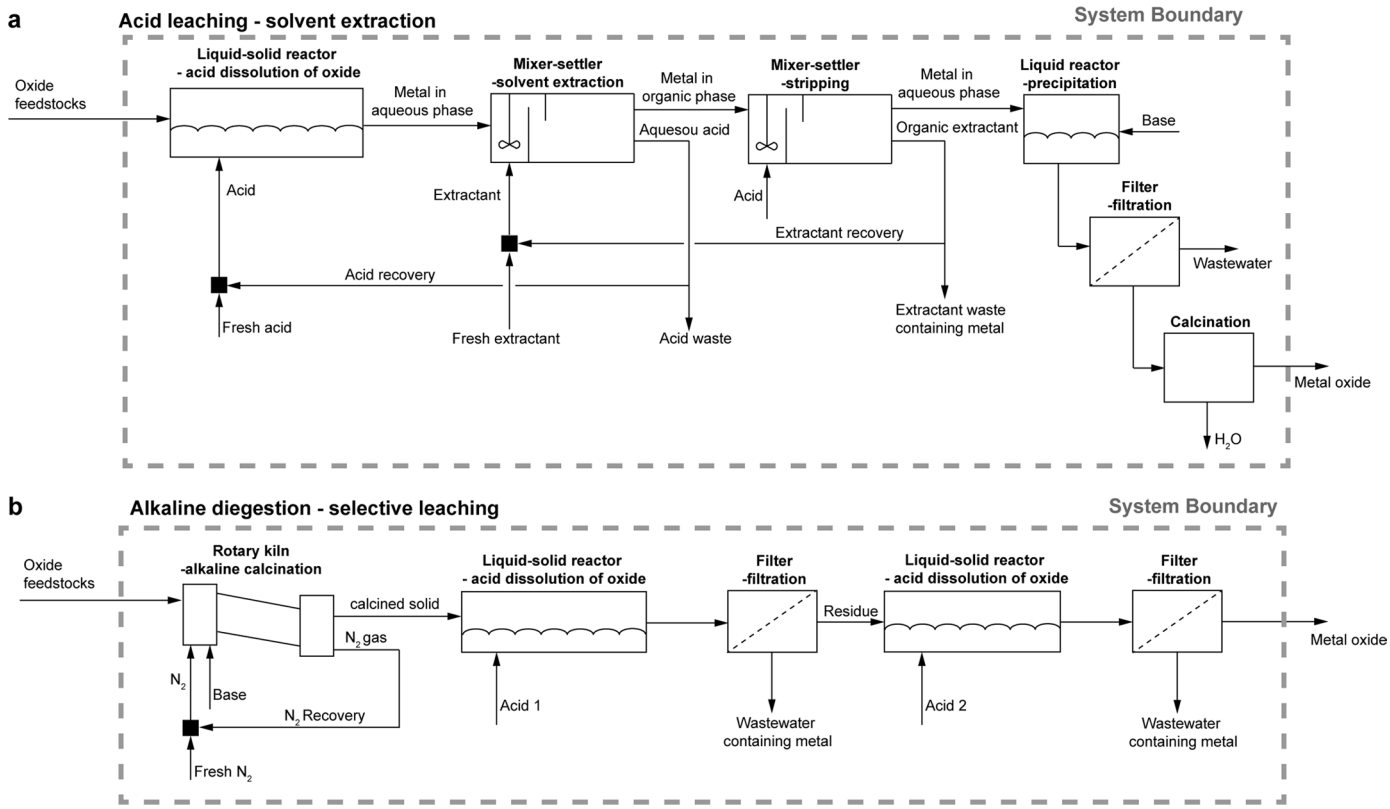

Extended Data Fig. 9 | Flowsheet of hydrometallurgical processes. (**a**) Acid leaching and solvent extraction. This process includes acid leaching of mixed metal feedstocks, solvent extraction for metal separation, stripping for metal recovery in aqueous phase, precipitation, filtration, and calcination to obtain the metal oxide product. (**b**) Alkaline digestion and selective leaching. This process involves alkaline calcination of mixed oxide feedstocks, acid leaching of the calcined materials, filtration, secondary acid leaching of the residue, and filtration to obtain the metal oxide product.

https://doi.org/10.1038/s44286-024-00125-2

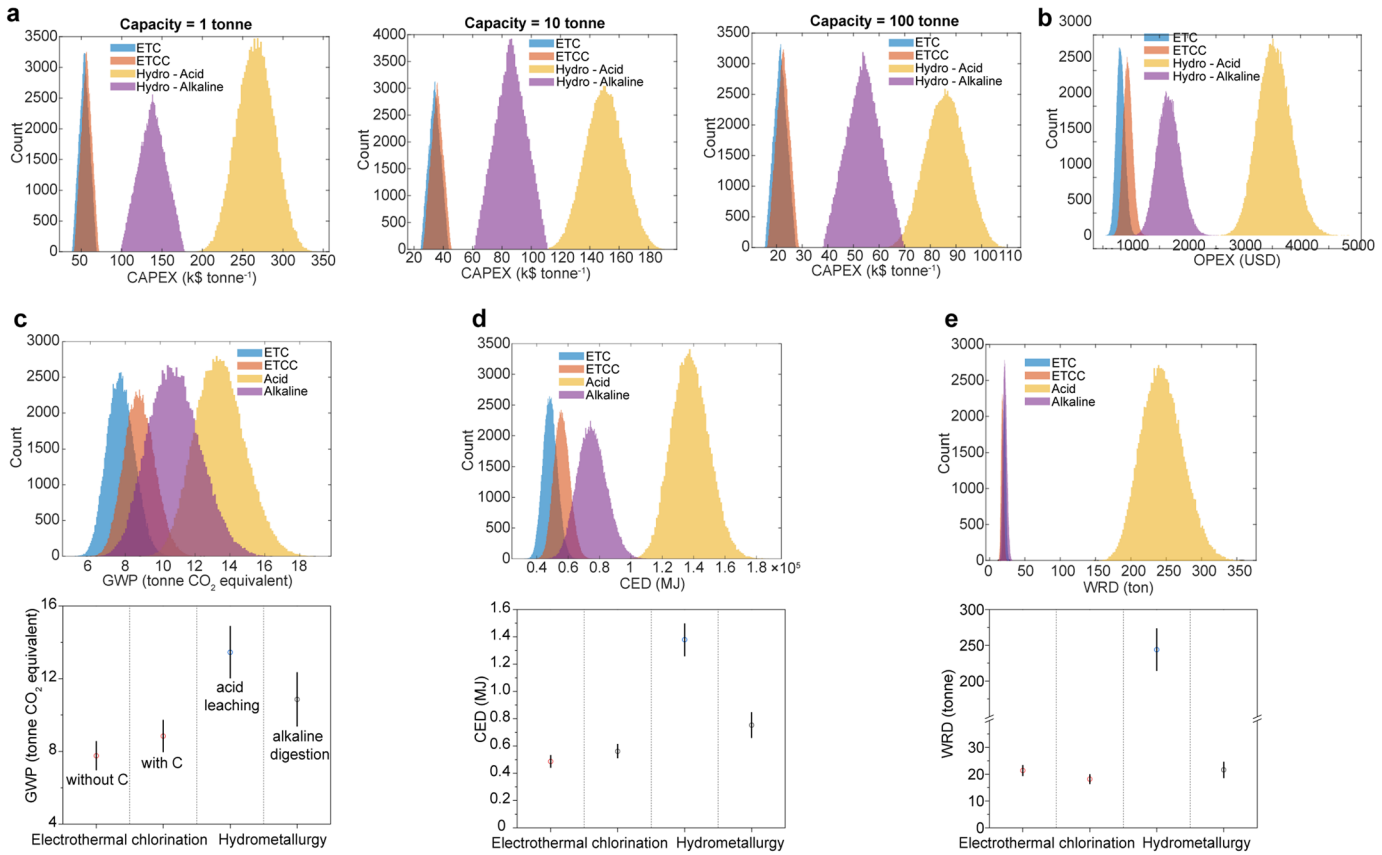

Extended Data Fig. 10 | TEA and LCA analysis. (**a**) CAPEX distributions for the four scenarios with different capacities at capacity = 1 tonne, 10 tonnes, and 100 tonnes. (**b**) OPEX distributions for the four scenarios. (**c**) Global warming potential (GWP) in CO_2 equivalent distribution (top), and the average GWP in CO_2 equivalent of four scenarios (bottom). (**d**) Cumulative energy demand (CED) distribution (top), and the Average CED of four scenarios (bottom). (**e**) Water resource depletion (WRD) distribution (top), and the average WRD of four scenarios (bottom). The error bars in **c**, **d**, and **e** represent one standard deviation. The functional unit of the LCA is the separation of 1 ton of mixed metal oxides. ETC, electrothermal chlorination. ETCC, electrothermal carbochlorination. Hydro – Acid, hydrometallurgy of acid leaching and solvent extraction. Hydro – Alkaline, hydrometallurgy of alkaline digestion and selective leaching.